AIRBORNE I. DAR OBSERVATIONS OF TROPOSPHERIC AEROSOLS DURING THE GLOBE PACIFIC CIRCUMNAVIGATION MISSIONS OF 1989 AND 1990

Robert 'I'. Menzies

David M. Tratt

Jet Propulsion laboratory

California institute of Technology

Pasadena, CA 91109

U.S.A.

Tel: 1-818-354-3787

March, 199S

AIRBORNE LIDAR OI3SERVA1"'1ONS OF TROPOSPHERIC AEROSOLS DURING 'l'] IE GLOBE PACIFIC CIRCUMNAVIGATION MISSIONS OF 1989 AND 1990

Robert T. Menzies and David M. Tratt

Abstract

Tropospheric and lower stratospheric aerosol backscatter profiles were obtained with an airborne backscatter lidar at 9.25 μm wavelength during the NASA Global Backscatter Experiment (GLOBE) missions in November, 1989 and May/June, 1990. The range of latitudes extended from 70 N to 62 S over the Pacific Ocean basin.

1. introduction

The Global Backscatter Experiment (GLOBE) airborne field campaigns in 1989 and 1990 included a suite of lidar and *in situ* instruments on the NASA DC-8 research aircraft which were used to provide atmospheric aerosol backscatter and microphysical data over the Pacific Ocean basin. 'l'he primary objectives of these Pacific circumnavigation missions were to characterize aerosol backscatter at infrared wavelengths in relatively pristine regions of the troposphere and to observe cloud effects on lidar profiling in support of NASA's analyses of Earth-orbiting Doppler wind lidar performance [*Bowdle, et aL,* 1991]. In addition it was considered important to use the opportunity to study aerosol microphysics and chemistry with on-board *in situ* instruments, and to establish intercomparisons between the lidar backscatter measurements and calculations of backscatter at the lidar wavelengths based on the contemporaneous *in situ* measurements. 'l'he. primary lidar wavelength for Earth-orbiting Doppler lidar analyses was the 9.1 μm wavelength of the CO_2 laser using the 0-18 isotope. The direct backscatter measurement instruments included a range-gated CO_2 lidar operating at 9.25 μm wavelength [*Menzies and Tratt, 1994],* a range-gated Nd:YAG lidar with three wavelength (0.53, 1.06, and 1.54 μm) capability [*Spinhirne, et al.,* 1991], and a focused cw laser backscatter instrument operating at 9.11 and 10.6 μm CO_2 laser wavelengths [*Rothermel, et al.,* 1996]. Each of these lidar instruments was carefully calibrated to provide quantitative aerosol backscatter coefficient data. Archived datasets have been generated by each of these instrument teams for the approximately 200 flight hours comprising the two flight series.

In this paper we present several products from the aerosol backscatter profile dataset obtained with the Jet Propulsion Laboratory (JPL) $C0_2$ lidar at the 9.25 μm

thermal infrared wavelength. The extensive latitudinal coverage in addition to the sampling of both eastern and western Pacific in the Northern Hemisphere resulted in a large dynamic range of observed aerosol backscatter coefficient, corresponding to a wide range of tropospheric air mass types and histories. The spatial scales of aerosol backscatter which have been produced range from 150 m in the vertical and 500 m in the horizontal (along the flight track) to large scale averages over 10-15 degree latitude and longitude bands, with vertical resolution of 500 m. The lidar data provide the opportunity to observe spatial characteristics and distributions of the boundary layer aerosol as well as distinct aerosol layers in the free tropical and extratropical troposphere, Mie theory calculations can be used to derive 9.25 μm optical thickness estimates for observed aerosol layers, based on the appropriate 9.25 μm lidar backscatter data. Aerosol model assumptions for the these calculations utilize the context provided by the corresponding Goddard Space Flight Center (GSFC) 0.53 μm and 1.06 μm lidar data, the dual wavelength Marshal] Space Flight Center (MSFC) backscatter data, and the in-situ aerosol instrument data.

When planning for the GLOBE missions began in the mid-1980's a major goal was extensive geographical coverage of the free troposphere, including the Southern Hemisphere. It was recognized that at least two missions were necessary in order to assess the magnitude and extent of seasonal variability. The modelling of Kent et al. [1984a,b] indicated generally lower aerosol backscatter and extinction at optical and infrared wavelengths over the Pacific than over the continents; however, data on aerosol properties over the Pacific was limited in geographical and temporal extent, and range of variability was a major question, The seasonal Asian dust effect was known to peak in spring in the Northern Pacific, based on data from the SEAREX (Sea/Air Exchange) network of island surface sampling stations (Uematsu, et al., 1983) and the Mauna Loa Observatory observations (Bodhaine, et al., 1981; Barrington, et al., 1983). The

November 1989 and May/June 1990 deployments provided the opportunity to observe the Northern Pacific near the extremes of the Asian dust transport cycle. $C0_2$ lidar measurements of aerosol backscatter coefficients in the mid-troposphere above Mauna 1.oa, Hawaii [Post and Cupp, 1992] and during westerly flow conditions above Pasadena, California [Menzies, et al., 1989] supported the belief that the Pacific free troposphere during the seasons of low Asian dust transport activity had significantly lower concentrations of optically active aerosol particles than the continental free troposphere. (The lidar measurements of aerosol backscatter in the troposphere above Boulder, Colorado in the early 1980's by Post [1984] clearly showed the influence of convective activity lofting surface and continental boundary layer aerosol into the mid-troposphere.)

During the succeeding years it has be-come apparent that the 1989-1990 period was one of relatively low stratospheric aerosol content and correspondingly low influx of stratospheric aerosol into the troposphere. This can be seen in the SAGE records reported by Brogniez and Lenoble [1991] and Hitchman, et al. [1994]. The lower stratospheric portion of the balloon-borne optical particle counter data covering a 20 year period, as reported by Hofmann [1993], also indicates relatively low concentrations of particles in the optically active size range in 1989-1990. The decade 1982-1992 measurements of optical depth above Mauna Loa, Hawaii, reported by Dutton, et al. [1994] clearly indicate a 10-yr low in the 1989-90 and 1990-91 fall-winter periods (outside the annual spring maxima due to dust transport). The JPL lidar 1984-1993 dataset of aerosol backscatter profiles also indicate an annual average minimum in the 1989-1990 period [Menzies and Tratt, 1995]. For the majority of the GLOBE observations the relative influence of surface and endemic tropospheric aerosol sources on the tropospheric aerosol budget was near its maximum,

These and other airborne lidar observations of aerosol backscatter coefficients and vertical structure over large geographical regions are useful in determining the degree

to which various tropospheric aerosol models used in radiative transfer calculations and in satellite radiometer derived aerosol properties are representative over the Pacific Ocean. They provide examples of the effects of transport and stability with respect to vertical mixing in the troposphere, which are relevant to modeling the influences of aerosol on climate. It is evident from analyses of effects of tropospheric aerosols on radiation that the overall warming or cooling, or influence on temperature lapse rate, depends on choice of aerosol model and such parameters as the assumed altitude profile and the wavelength dependence of the extinction coefficient [Coakley, et al., 1983].

2. INSTRUMENTATION

The airborne CO_2 coherent lidar which was used for aerosol vertical profile measurements on the GLOBE missions has been described previously [Menzies and Tratt, 1994]. The lidar transmitter is a single-frequency injection-seeded CO_2 laser, tuned to the 9.25 μm laser line, and the receiver employs heterodyne detection. It is a design which is used for Doppler wind measurements; however in this case the aerosol backscatter intensity measurement was the objective. The lidar receiver bandwidth is 10 MHz (approximately 3×10^{-3} rim). The installation in the DC-8 permitted either nadir or zenith pointing, depending on the circumstance. During the transit flights when the aircraft was at typical cruise altitudes (usually 8 km, occasionally as high as 13 km) the lidar was operated in the nadir mode the majority of the time. A "dead zone" of about 400 m existed between the lidar and the first range gate of valid data.

Calibration issues for a thermal infrared wavelength backscatter lidar such as this have been discussed in Kavaya and Menzies [1985]. The lidar is calibrated using a remotely deployed hard target whose reflectance characteristics are referenced to laboratory standards in order to produce tropospheric and lower stratospheric aerosol

backscatter profiles in absolute units. The calibration methodology and the sensitivity of coherent detection at these relatively long infrared lidar wavelengths is well suited for tropospheric and lower stratospheric measurements even in conditions of low aerosol loading. The long wavelength and high spectral resolution of the lidar result in the small molecular Rayleigh backscatter signal which is within the receiver passband being below the receiver noise level throughout the troposphere. In contrast at visible and near infrared lidar wavelengths the aerosol backscatter is a small fraction of the Rayleigh backscatter in clean conditions,

In addition to the independent hard target ca ibration exercises, the JPL airborne backscatter lidar participated in instrument intercomparison flights in the neighborhood of the NASA Ames Research Center. The chief intercomparisons were among the JPL lidar, the airborne MSFC focussed cw CO_2 laser instrument, and the ground-based NOAA Wave Propagation Laboratory (WPL) CO_2 lidar located at the Ames Research Center. The JPL and NOAA lidars generated vertical profiles of aerosol backscatter, while the MSFC instrument data were collected during ascent and descent as well as the multiple flight level overpasses of the Ames (Moffett Field) area. The data were obtained from surface to 12 km altitude, providing the opportunity to intercompare over a wide dynamic range of aerosol concentration (approximately three orders of magnitude in backscatter coefficient). The measured backscatter coefficients and vertical structure observations were consistent among the three instruments. The intercomparison exercise and results are described in more detail in Menzies and Tratt [1994].

The lidar data obtained during the GLOBE flights have been processed and converted into vertical profiles of atmospheric backscatter in calibrated absolute units, using two horizontal resolution modes, each with vertical resolution of approximately 100 m. The horizontal resolution (along flight track) of the higher resolution mode, corresponding to IO-shot averages, is typically near S00 m, depending on the aircraft

cruise speed. Display plotting of the data in this mode permits the recognition of both vertical layering and the extent of horizontal homogeneity at a given altitude. This is useful for an assessment of the relevance of spatial averaging over larger scales. It is also useful for identification of cloud extent and discrimination between optically thin cloud and aerosol. The lower resolution mode corresponds to 400-shot average profiles, resulting in typical horizontal resolution of 20 km. This mode is used for the higher sensitivity necessary to extract backscatter coefficients in the relatively clean atmosphere.

3. RESULTS AND DISCUSSION

'l'he flight tracks for both the November 1989 (GLOBE 1) and May/June 1990 (GLOBE 2) missions are depicted schematically in **Figure 1. The** latitude range for each mission was approximately 70° N to 60° S. Local flights were conducted in the vicinity of Hawaii and Japan during both missions, The three Japan local flights in November 1989 were primarily over the islands, with correlative measurements among ground-based lidars having a high priority. In June 1990 the single Japan local flight was used to concentrate on measurements southeast of Japan to further study the multiple layers of elevated aerosol which were observed on the approach to Japan during the previous Darwin, Australia to Tokyo flight leg. Two local flights out of Melbourne, Australia were conducted off the south coast of Australia during GLOBE 1, and a single local flight out of Christchurch, New Zealand was conducted during GLOBE 2, extending to the east and south of New Zealand. The local flights generally included flight legs at a variety of altitudes, while during the transit flights the aircraft generally remained at cruise altitudes between 8 km and 10 km, occasionally ascending to altitudes as high as 13 km in order to avoid cirrus at the normal cruise altitudes.

The GLOBE 2 lidar profile dataset is significantly larger than the GLOBE 1 dataset. The laser transmitter pulse-repetition frequency was 25% higher during the GLOBE 2 mission. In addition the data collection was more efficient during the second flight series due to less "down time" devoted to instrument performance diagnosis, Consequently the GLOBE 2 data can be processed with better resolution of spatial structures, as discussed later.

Size Range of Lidar Active Aerosol I'articles

Analogous with the term "optically active" aerosol particles (radii $> 0.15\,\mu m$) commonly used by aerosol investigators (e.g., *Hofmann [1993]),* it is useful to first understand what particle size range is dominating the lidar backscatter for the 9.2S μm lidar wavelength for various tropospheric conditions. Using the common Mie scattering assumption of spherical particles (which is a crude approximation for certain classes of tropospheric aerosol, e.g., crustal material), the aerosol backscatter coefficient $\beta\,(m^{-1}\,sr^{-1})$ at the lidar wavelength λ can be expressed in erms of the particle size distribution, n *(r)dr* and geometric cross section πr^2, as

$$\beta\,(180°) = (4\,\pi)^{-1} \int_0^\infty (\pi r^2)\, Q_{sca}\,(\lambda,r) P(180°) n(r) dr \qquad (1)$$

where $Q_{sca}(\lambda,r)$ is the scattering efficiency for a particle of radius r, and $P(180^o)$ is the phase function at the 180° backscatter angle.. In the Rayleigh limit of small values of the size parameter, $2\pi r/\lambda$, the product of geometric cross section and scattering efficiency increases as r^6. For the lidar wavelength of 9.25 μm, the effective exponent for particles with radii between 0.2 and 1 μm lies between S and 6. Most analyses of the tropospheric aerosol size distributions have used multimode forms of the lognormal size distribution

$$n(r) = \frac{No}{\sqrt{2\pi}\, r \ln s} \exp\left(-\frac{(\ln(r/r_g))^2}{2(\ln(\ln s))^2}\right) \quad (2)$$

where No is the total number concentration, r_g is the median radius, and s is the geometric standard deviation, or multimodal variations of this form. The "effective radius" for the monomodal lognormal distribution is

$$r_{eff} = r_g \exp(2.5(\ln .)2), \quad (3)$$

Pueschel et al. **[1994]** used multi-component lognormal distributions to fit portions of their particle counter data obtained during the G] .OBE missions. Using their best fit values of r_g ands in equation (l), modified slightly in accordance with correction factors described by *Cutten et al.* [1996] to improve the representation of the large particle tail, one can conclude that in the typical DC-8 cruise altitude (8-12 km) regions of the troposphere (excluding those layers containing elevated aerosol mass dominated by material of continental origin), the components which dominate the lidar backscatter are relatively narrow (s - 1.5), with the modal radii being 0.1-0.2S pm, and that within these modes the particles with radii in the 0.25 -0.8 μm range contribute the most to the lidar backscatter coefficient. (*Srivastava et al. [1992]* provide an example of $d\beta/d\log r$ for 9.1 μm wavelength and a very similar lognormal size distribution, r_g = 0.15 μm, s = 1.S, showing a rather broad peak at particle radii near 0.4-0.S pm.) Within the extensive dust layers observed at northern subtropical and mid-latitudes during the GLOBE 2 (May/June 1990) mission, the range of particle radii which most effectively contribute to the lidar backscatter is 0.5-2 μm. The lidar β is a sensitive function of s in the lognormal fit to a size distribution, since s governs the extent of the large-particle tail

Among the standard physical quantities derived from the aerosol size distribution, the β measured by this lidar is most closely correlated with aerosol mass per unit volume, the mass also being dominated by the larger particles in the size distribution.

As an example of a representative link between a GLOBE "baseline" aerosol size distribution and 9.25 μm backscatter, we can consider the mean values of the (2-component) lognormal fit parameters for a large number of particle counter samples taken during "background" (no evidence of cloud or elevated aerosol layer effects) conditions at 8-10 km altitude [*Pueschel, et al.*, 1994]: N_{01} = **20** cm^{-3}, r_g = **0.06** pm, u = 1.5; N_{02} = 0.6 cm^{-3}, r_g = 0.2 μm, σ = 1.4. As stated above, the component of larger mode radius dominates the lidar backscatter. Assuming an aerosol of 75% liquid sulfuric acid solution, which is often dominant in the upper troposphere away from continental influence *[Sheridan, et al., 1994; Yamato and Tanaka, 1994],* the computed lidar backscatter coefficient is 1.4 x 10^{-11} m^{-1} sr^{-1}.

Derivation of Mean Values of Aerosol Backscatter over Various Spatial Scales

The data set of aerosol backscatter profiles with 150 m vertical and 20 km horizontal resolution have been binned and averaged over larger spatial scales to create various data products. For the purposes of averaging, lognormality of the appropriate set of backscatter values at a given altitude. is assumed; hence geometric means are calculated. The lognormality of aerosol backscatter samples at a given altitude produced by ground-based lidar profiling has been discussed previously [*Post and Cupp*, 1992, and references therein]. The lognormality property can be deduced by considering the important growth and scavenging processes which act on the optically active aerosol particle population as multiplicative processes which can be modelled with rate equations. The ground-based profiles used to point out the lognormality of aerosol backscatter coefficient distributions at fixed altitudes were typically "snapshots" taken

over the course of a few minutes, separated by hours or days. This implies that each ground-based profile represents an intrinsic average over horizontal scales of 100 m to 10 km depending on the velocities with which the air masses advect by the fixed lidar site. The collections of data points comprising the lognormal β distributions represented data collection periods of several weeks, typically. The airborne lidar profiles are intrinsic averages over about 20 km, some nearly contiguous, others separated by gaps of more than 100 km due to cloudiness or viewing intervals in the opposite direction.

Fixed-altitude data sets from various GLOBE flights have been sorted and plotted in the familiar log β vs. cumulative probability format to check the lognormality assumption, These data sets cover horizontal scales ranging from a few hundred km to about 2000 km. The fixed-altitude data sets fit the lognormal distribution much more closely than the normal distribution. Figure 2 includes a set of backscatter coefficients measured during clear sky conditions at 600 m above sea level during the GLOBE 1990 flight between Tahiti and Christchurch, New Zealand. Each data point represents an average over a cloudless segment along the flight track of about 20 km distance. The flight track extent corresponding to this dataset is 2000 km. This is typical of fixed altitude aerosol backscatter data, showing lognormal behavior except for a few data points at the high end and the familiar downturn at the low end. The downturn is a common result of dropout compensation [*Post and Cupp*, 1992; *Tratt and Menzies, 1994].* Dropouts occur when the backscatter signal at a particular altitude is near or below the lidar noise level, eliminating the possibility of an accurate measurement. The usual assumption of the dropout compensation algorithm is that the lidar sensitivity at a given altitude is a constant and the lost values of backscatter are all below the lowest measured value of backscatter for that altitude. Small variations in the lidar sensitivity (or "noise-equivalent backscatter coefficient") from shot to shot or among the profiles (resulting from aircraft altitude changes) can result in the lowest data points being

placed at cumulative probability levels which are biased high, thus contributing to the downturn characteristic. A percentage of the lower and upper data points are typically excluded in the least-squares line fitting for determination of the geometric mean and standard deviation in order to eliminate those data points in the downturned tail of the distribution.

The conclusion of the cumulative probability distribution studies is that data points in a fixed altitude bin are sufficiently close to the lognormal characteristic to permit the use of the geometric mean for averages. In some cases it is apparent from a plot of data points representing a large horizontal scale (e.g., a 10^{o} latitude band) that the set is composed of distinct populations, which can be separated for individual lognormal fitting. The combined mean is used for display of large-scale patterns, such as the examples described next.

Latitude and Longitude Cross-Sections

The profile data from the transit flights of each of the GLOBE missions were spatially averaged over 500-m altitude intervals and 10-degree (GLOBE 1990) or 15-degree (GLOBE 1989) bands of latitude in order to create color-coded latitude-altitude contour plots of geometric mean aerosol backscatter covering the range from approximately 60° S to 60° N. (The data from the transits over the Australian continent were not included.) In a similar manner a northern mid-latitude longitude-altitude contour plot was generated from GLOBE 1990 data, extending from 135 E to 120 W longitude. For each resolution element a lognormal fit was calculated, and the geometric mean backscatter value was used as input to the contour plot.

These plots provide an overall impression of the altitude dependence of aerosol backscatter through the troposphere and the distinctions which appear between the two hemispheres during the May/June period of the GLOBE 1990 flights versus the

November GLOBE 1989 flights. The data processing algorithm which was developed for this purpose included various means of filtering out cloud "contamination" in order to produce unbiased aerosol backscatter contours. Both high resolution lidar data and data from the nadir viewing video camera onboard were used to identify cloud layers and set appropriate discriminants for each flight dataset.

Figures 3 and 4 are the color-coded latitude-altitude contour plots for the GLOBE November, 1989 and May/June, 1990 missions, respectively. A few explanatory comments regarding the data gathering and the contour plotting are in order. White indicates a region where there is insufficient valid data. This can be due to the presence of extensive clouds, low SNR (signal-to-noise ratio), or insufficient sampling of a portion of the atmosphere. Since the lidar sensitivity to aerosol backscatter decreases with increasing range, the noise-equivalent β (backscatter coefficient) is altitude dependent. The various latitude bands were not sampled evenly due to the various flight track headings. Thus the sensitivity depends on both latitude and altitude. 'l'he black borders contiguous to these regions are an artifact of the contouring algorithm, not a property of the atmosphere. Since the lidar operated in either a nadir or zenith pointing mode, the dead zone of no valid data within 400 meters of the aircraft resulted in a relative dearth of data near the cruise altitude. In Figure 3 the region of no data at 9-10 km in the equatorial latitudes is due to insufficient sampling, caused by a combination of the dead zone effect and lidar instrumental checks which precluded data gathering. 'I'he regions for which $\log\beta < 11.0$ are near the lidar sensitivity limit, and the associated random uncertainty in the calculations of the average aerosol backscatter for these regions is about +/- 3 dB. The blank region between 2 km and 5-6 ktn at the extreme south latitudes is due to the presence of extensive but often tenuous cloud cover, with low enough opacity at the 9.25 μm wavelength to permit measurement of boundary layer aerosol backscatter below. In Figure 4 the data gaps in the 8-9 km altitude region are

due to the combination of low aerosol backscatter conditions and insufficient sampling adjacent to the aircraft cruise altitudes. The blank regions in the tropical upper troposphere are partially due to extensive cirrus, reducing the opportunities for clear air aerosol measurements, although the relatively few clear air profiles obtained in this region indicated low aerosol backscatter conditions. The blank regions at the extreme north latitudes are due to the presence of extensive cloud cover, often optically tenuous but sufficient to negate the measurement of aerosol profiles. The aerosol backscatter column projecting into the lower stratosphere near 20° N very likely does not represent a localized aerosol plume as much as an extraordinarily large number of upward looking "clear sky" lidar samples at this latitude.

A significant feature of the Nov/Dec 1989 latitude cross section is the rather symmetric appearance with respect to north and south latitudes, with relatively low optically active aerosol content in the tropical northern hemisphere, at altitudes above the boundary layer. Even the boundary layer aerosol column is significantly reduced in this region, with a minimum near 5°- 10° N latitude. The thinning of the planetary boundary layer (PBL) corresponds with the location of the Intertropical Convergence Zone (ITCZ) at the longitude of the Hawaii to American Samoa transit flight, which is consistent with the strong cumulus convection acting as a sink of PBL mass and thereby limiting the PBL depth [*Randall, et al.*, 1985]. The low optically active aerosol content in the tropics is due to the effective convective. entrainment and in-cloud aerosol particle scavenging in the large convective cumulus structures. *Clarke* [1993] observed both very low aerosol mass and very high small particle (UCN, or ultrafine condensation nuclei) number densities at flight level during the GLOBE flight transits of the equatorial zone. The UCN particles, with diameters ≤ 15 nm, are too small to nucleate droplets in clouds. The low efficiency of wet deposition combined with low aerosol surface area available

for heterogeneous coagulation results in relatively long lifetimes for these particles in the middle and upper tropical troposphere..

The tongue of relatively high β values reaching up to 5-7 km altitude which is apparent in the 35°- 40° N region is due to the observations in the western Pacific in the vicinity of Japan and in the eastern Pacific within 300 km off the coast of California. Observations in the eastern Pacific on the leg from Moffett Field, California to Hawaii indicated a transition to a low aerosol mass environment beyond the first 300 km, with lidar β values in the mid-troposphere dropping to near $10^{-11}\,m^{-1}\,sr^{-1}$.

It is apparent from Figure 3 that the lower stratosphere is unusually devoid of aerosol mass, as discussed earlier, with lidar β levels being near or below $10^{-11}\,m^{-1}\,sr^{-1}$ at mid- and high latitudes when the aircraft altitudes were within 3 km of the tropopause. This is not surprising in view of the volcanic activity context previously discussed.

'l'he May/June 1990 latitude cross section shown in Figure 4 shows an evident hemispheric asymmetry in contrast to the Nov 1989 latitude cross section. The more detailed individual flight data, combined with data from the on-board LOPC (I .aser Optical Particle Counter) [Clarke, 1993] and focussed-cw CO_2 laser sensors [*Srivastava, et al., 1995],* indicate that the high aerosol content in the northern extratropical latitudes is largely due to layers of Asian dust being advected across the Pacific at various altitudes. The seasonal transport of Asian dust across the northern Pacific to Hawaii is well documented (e. g., *Bodhaine, et al., [1981]; Darzi and Winchester, [1982]; Parrington et al.,* 1983]; *Dutton et al.*, [1994]). These extensive measurements are based on either *in situ* sensors or sun photometer optical depths from the Mauna Loa site.

A longitude cross section compiled from GLOBE 2 Northern Hemisphere extratropical latitude data (excluding the data over Alaska) is shown in Figure 5. The decrease in aerosol column integrated backscatter as well as the subsidence of the upper

boundary transition from elevated aerosol backscatter to clean "background" troposphere backscatter levels in going from east to west is consistent with the strong Asian source and the scavenging and sedimentation of the aerosol as it is advected by the westerlies across the Pacific. The lifting of the aerosol column near 160° W longitude coincides with the longitude of the Hawaiian islands and may be an artifact of the use of Hawaii as a way point in both north-south and east-west traverses of the Northern Hemisphere Pacific.

As can be seen in Figures 4 and 5 the Asian dust effects extend to altitudes near 12 km, reaching the tropopause at approximately 40° N. *Kent et al.* [1995] have also observed springtime lifting of tropospheric aerosol in the northern hemisphere up to the tropopause above 40° N latitude, based on a multi-year analysis of zonally averaged and seasonally averaged SAGE II solar occultation data at 1 pm. It is likely that the zonal sector including eastern Asia and the western Pacific is responsible for the observation in the zonally averaged data.

The lower stratosphere in spring, 1990 contains much more aerosol mass than in fall, 1989, particularly in the southern hemisphere, as seen in Figure 4. Lidar aerosol backscatter coefficients reach levels slightly above $10^{-11}\,m^{-1}\,sr^{-1}$ at some locations in the 15-20 km region. The aerosol plume from the Kelut (8S, 112E) eruption of February, 1990 is the dominant cause. The Kelut effect is also evident in the SAGE spring 1991) data depicted in *Trepte, et al. [1993]* and *Kent et al.* [1993]. The SAGE data clearly indicate that the plume had dispersed primarily into the southern hemisphere, As portions of the plume subsided to altitudes near the subtropical tropopause ("tropopause break" region) it is likely that cross-tropopause mass exchange occurred, raising the upper tropospheric aerosol content above the corresponding fall, 1989 level, *Kent, et al.* [1995], using a multi-year analysis of SAGE 11-μm extinction data and a technique for separating out the volcanic aerosol component in the upper troposphere, observe the

transfer of lower stratospheric volcanic component into the upper troposphere poleward of 40°. It appears from Figure 4 that transfer of Kelut material into the upper troposphere is taking place poleward of 20° S.

A sharp latitude gradient aerosol abundance is observed in the May/June 1990 cross section between 10-15 N latitude at lower and middle altitudes in the free troposphere, evidence again of the effectiveness of the tropical cumulus convection as a sink for the aerosol particles in the lidar-active size regime.

The southern extratropics contained less aerosol in the free troposphere in the May/June 1990 period than in Nov 1989. The seasonal cycle in the southwest Pacific has been noted by *Kristament, et al.* [1993], The GLOBE lidar data indicate that the amplitude of the seasonal cycle is much greater across portions of the north Pacific.

The effect of the tropical cumulus convection on the boundary layer thickness in the ITCZ region also appeared in the May/June 1990 transit flights across the equatorial latitudes. A significant reduction in PBL aerosol column also appears in the vicinity of 30° S latitude. This latitude region was traversed in the western Pacific near New Zealand, as indicated in Figure 1.

Layers of Elevated Aerosol Backscatter Outside the Equatorial Belt

The smoothing and contouring processes used to produce Figures 4 and S shroud the fact that the elevated aerosol backscatter observed particularly in the northern hemisphere spring was observed in distinct layers, often separated by very clean air. These layers were observed to have a sharp, well-defined low latitude boundary. The transition between the equatorial region of very low aerosol mass and the subtropical latitude region of elevated aerosol layers at mid- and upper tropospheric altitudes occurred near 15° N latitude on both the Hawaii to American Samoa (May 20, 1990) and

Darwin to Tokyo (May 31, 1990) flights. Figures 6 and 7 are examples of the transition profiles corresponding to these two flights. The aerosol layer with a broad peak near 5 km in Figure 6 was observed at 14° N latitude flying south from Hawaii, while the profile observed about thirty minutes later at 10.5° N indicates only a small remnant of the layer, This thin layer and its neighbors above it decreased further soon thereafter. The narrower layer with peak near 2.5 km is no longer distinctive at 10.5° N, the aerosol backscatter level having dropped by over an order of magnitude. The boundary layer aerosol mass has decreased significantly also. On the May 31 flight to Japan the profiles of Figure 7 indicate the transition between a composite profile based on observations in the 12°-140 N latitude region and another composite profile based on observations in the 15°-160 N latitude region. Very clean lower and middle tropospheric conditions below 15° N suddenly changed with the obvious appearance of a thick layer with a sharp base . just below 6 km, As the aircraft continued to pass above this layer it grew in thickness and in peak backscatter to a level above 10^{-8} m^{-1} sr^{-1} at 20-22° N latitude. As the flight progressed through the 20-30° N latitude band the column integrated lidar backscatter between flight level (8 km) and the top of the PBL was measured at 1-3 x 10-5 sr^{-1}. (A few examples of the lidar observations of these layers are found in *Menzies and Tratt [1994].)* By comparison the maximum observed integrated backscatter through the Pinatubo aerosol column over the Pasadena, California location (34° N) was 3 x 10^{-5} sr^{-1}.

It is of interest to estimate the 9-μm opacity through these observed elevated aerosol layers. Data taken over a range of altitudes during a separate flight in the region southeast of Japan, combining lidar observations with the onboard *in situ* particle microphysics observations, support an aerosol mode] with Asian dust as the predominant mass and lidar backscatter component. Using lognormal fits to the observed size distributions, with r_g = 0.5-0.6 pm, s = 1.6, N_0 = 0.3- 1.0 cm^{-3} near the peaks of the layers, the computed extinction-to-backscatter ratio at the 9.25 μm lidar wavelength is

near 10^2. Thus the optical depths (from aircraft altitude to top of PBL) through the most pronounced dust layers were approximately 1-3 x 10^{-3}.

Geometric Mean Tropical and Extratropical Profiles

The lidar data were sorted into three latitude bands of 40° width, the 60° S to 20° S, 20° S to 20° N, and 20° N to 60° N bands corresponding to SH extratropical, tropical, and NH extratropical groups, respectively, in order to produce geometric mean profiles representing these regions, for the fall, 1989 and spring, 1990 GLOBE missions. Figure 8 depicts the spring, 1990 profiles for each of these latitude bands. In each case the rapid decrease in aerosol backscatter with altitude up to 3-4 km is indicative of the source of lidar-active aerosol particles in this region being convective mixing from below. The tropical profile is bifurcated in order to discern the effect of removing the contribution from 15°-200 N, which was observed as a transition zone with aerosol properties more like the extratropical northern hemisphere. The removal reduces the "tropical" aerosol backscatter profile most significantly in the middle troposphere. This profile, representing 20° S to 15° N, is compared with the November, 1989 tropical profile in Figure 9. The tropics as observed in the GLOBE 1989 mission presented a middle and upper troposphere most devoid of aerosol mass, with aerosol backscatter levels equivalent to the lowest observed in the 10-yr history of middle and upper tropospheric aerosol backscatter profiling above the Pasadena, California site [*Tratt and Menzies*, 1995]. The May/June 1990 tropical profile, although representing an air mass relatively devoid of aerosol mass, differs significantly above 6 km altitude, Reviewing Figure 4 it appears that the source of the aerosol layers from the northern extratropics contributes to the observed increase in the 6-11 km region, while stratosphere-troposphere mass exchange particularly at southern latitudes contributes to an upper

tropical troposphere enhancement. In contrast the stratosphere above was very clean in the fall, 1989.

It is apparent from Figures 8 and 9 that the aerosol backscatter at the lidar wavelength covers a wide dynamic range, from typical boundary layer values down to levels observed in the southern hemisphere extratropical fall (May/June, 1990) and in the tropics at middle and upper tropospheric altitudes. The aerosol in the latter atmospheric air masses provide examples of an aerosol backscatter background mode [*Rothermel, et al.,* 1996], The sources of mid-altitude aerosol particles in the lidar-active size range at southern mid-latitudes are expected to be relatively small in the austral au t umn [*Kristament et al., 1993],* and the wet removal processes for this size range [*Prospero, et al. 1983],* e.g., mid-latitude convective cells and frontal systems, effectively purge the middle troposphere. 'J'he wet deposition removal processes in the tropics associated with the large cumulus structures effectively removes the particles in the mid-troposphere *[Clarke,* 1993; *Rehfeld and Heimann, 1995],* whereas the lifetimes of aerosol particles in the lidar-active size range are expected to be much longer in the relatively dry subtropics [*Rehfield and Heimann,* 1995].

Variability of Boundary Layer Aerosol Backscatter

The statistical distributions of the boundary layer aerosol backscatter datasets have been given particular attention, noting that the lidar data are indicative of aerosol mass within the boundary layer and aerosol column mass through the thickness of the boundary layer. The lidar backscatter values can be linked to surface wind speed using a model to relate the aerosol number density and size distribution to wind speed [*Gathman,*1983; *Gerber, 1991].* The boundary layer thickness and aerosol column mass are indicative of e.g., surface heating and the cumulus convection sink as well as surface

winds and are useful benchmarks for model parameterizations of the PBL [e.g., *Randall, et al.,* 1985].

The latitude-altitude cross sections represented in Figures 3 and 4 indicate significant latitude dependence of PBL aerosol backscatter coefficient and column-integrated aerosol backscatter. The minimum in the 0^{o}-10^{o} N band, the maxima in the subtropical latitude regions, and the rise in thickness near 60° S are common to both the Nov. 1989 and May/June 1990 periods.

The lidar profile data (100-sec time average profiles) have been sorted into various altitude bins and grouped according to latitude band, time period, and flight in order to plot the data as gaussian cumulative distributions (as in Figure 2) and observe statistical properties. Cloud filters in the processing algorithm exclude those profiles for which clouds exist at or above that altitude. High resolution profile data (2-see average, corresponding to 400-500 m resolution along track) as well as nadir-pointing video camera images have been used to discern the. presence of clouds within the 100-sec time periods corresponding to these profiles and validate the cloud filters in the. algorithms.

Examination of the tropical PBL data indicates two distinctly different aerosol backscatter properties which can be identified with separate geographical regions. The lidar backscatter data in the bin centered at 2S0 m altitude above sea level within the 20° S to 20° N tropical latitude band are plotted in cumulative distribution format in Figure 10. The mean value β_m is approximately $2 \times 10^{-8}\ m^{-1}\ sr^{-1}$. The data follow a curve which is indicative of two lognormal populations, the lower backscatter population covering the $\log\beta$ range from about -9 to -8, and the upper population covering the range from approximately -8 to -7, starting near the 40th percentile. A more detailed study of the individual profiles indicates that the lower backscatter population comes from the 0°-10° N band of the Hawaii to American Samoa flight and the 5° S to 20° N band of the Darwin to Tokyo flight. This distribution, with $\beta_m = 5 \times 10^{-9}\ m^{-1}\ sr^{-1}$ is plotted in

Figure 11. These also correspond to the regions of minimum PBL (geometric) thickness. The very low PBL aerosol backscatter conditions were observed over a much wider latitude band in the western Pacific "warm pool" region, well known as a broad region of rising motion in the so-called Walker circulation. in contrast the PBL aerosol backscatter was observed to be distinctly higher at the southern latitudes covered by the American Samoa to Tahiti flight and outside the 0-10° N band in the Hawaii to American Samoa flight. The distribution from these regions, with $\beta_m = 3 \times 10^{-8} m^{-1} sr^{-1}$, is plotted in Figure 12. The width of this distribution is notably small, with s = 1.6.

'l'he corresponding PBL (2S0-111 altitude) aerosol backscatter cumulative distributions for the northern extratropical and southern extratropical latitudes are plotted in Figures 13 and 14. The distributions are quite similar in mean value and spread, and similar to the distribution for the tropics outside the regions of intense cumulus convection activity. To reiterate each of these data points represents cloud-free conditions from the aircraft altitude to the surface over a horizontal scale of about **20** km. The PBL directly beneath cyclonic storms or other unstable conditions for which the surface winds are generally strong is not represented in these data.

The lidar backscatter coefficient from the PBL aerosol can be linked to surface wind speed through a model such as the semiempirical model of *Gathman [* 1983], more recently modified by *Gerber* [1991]. Gathman's model is based on a dataset of over 800 measurements of aerosol size distributions combined with corresponding meteorological parameters measured nominally 15 m above the ocean surface. The size distribution of the PBL aerosol particles is modeled as a sum of three lognormal distribution components, each with a geometric mean radius which contains a multiplicative RH (relative humidity) growth factor. Assuming an RH range of 70% to 98%, which includes a wide range of conditions, we find the corresponding range of particle radii. The first component corresponds to an aged continental component with geometric mean

radius of $0.05 < r_g < 0.085$ μm over this RH range. The second component is a distribution of sea-salt particles driven by the surface wind, averaged over a diurnal period, with geometric mean radius of $0.35 < r_g < 0.8$ μm over the same RH range. The third component represents the distribution of gust-driven large sea-salt particles, with corresponding geometric mean radius $3 < r_g < 6.5$ μm range. For lidars at wavelengths from mid-visible to thermal IR the second component dominates for wind speeds from 3-30 m s^{-1}, except possibly in coastal zones or downwind from major dust sources. Using Eqn (1) to describe the dominant component of the Gathman model as modified by Gerber, the functions] dependence of the particle number density (cm^3) on wind speed is given as

$$N_2 = 3.3(\tilde{w} - 2.2) \quad \textbf{(4)}$$

where r_g is replaced by fr_g, f being the RH I growth factor,

$$f = \left[\frac{K_1 - S}{K_2(1 - S)} \right]^{1/3} \quad \text{(s)}$$

where the saturation ratio S = RH/100, and $K_1 = 1.83$, $K_2 = 5.13$.

Measurements of aerosol backscatter coefficient near the surface at a single lidar wavelength must be supplemented with RH measurements or estimates in order to deduce the surface wind speed, However combined Nd:YAG and CO_2 lidar measurements can be used to deduce both wind speed and RH, using this model, A limited set of combined GLOBE lidar PHI, backscatter coefficients from northern subtropics] latitudes in the western Pacific [*Menzies and Tratt, 1994]* have been used to compare with model predictions, resulting in retrieved wind speeds in the 4-7 m s^{-1} range

with relatively low RH values. These compare well with the May and June 1990 monthly mean surface wind speed products from the special sensor microwave imager (SSMI) [*Halpern, et al.*, 1993], plotted in Figure 15 vs. latitude, at 135° E longitude. Further investigation of wind speed retrievals using these multi wavelength lidar datasets is planned.

Variability of Free Troposphere Aerosol Backscatter

'l'he latitude and longitude cross sections exemplified in Figures 3-5 provide a good indication of large scale spatial variability for the fall and spring seasons. These contour plots are composed from geometric mean β values, as stated earlier. It is of interest to have in addition an indication of the range of aerosol backscatter coefficients within the averaging cells or within adjacent groups of cells. Distributions of aerosol backscatter datasets at particular altitudes have been analyzed for portions of the GLOBE flights. The β distributions have also been plotted (in cumulative distribution format) for the tropical, northern extratropical, and southern extratropical bands used previously, at particular fixed altitudes up to 10 km, with best fit lognormals applied. As an example the GLOBE 1990 northern extratropical distribution at the altitude bin centered at 5.2S km is plotted in Figure 16. This relatively large range of β values is greatly influenced by convection and transport processes. The fit to this distribution produces $\beta_m = 7 \times 10^{-10}\ m^{-1}\ sr^{-1}$ and $s = 3.4$. Not all the β distributions can be fitted as well as this example with a single lognormal. We have found that particularly the GLOBE 1990 northern extratropical datasets at the higher altitudes (above 6 km) commonly exhibit two or more modes, appearing to be correlated with the degree to which the aerosol population contains particles of land surface origin. **in** these cases the geometric mean remains a useful statistic; however a single standard deviation can be misleading, Tables 1 and 2 contain listings of parameters resulting from best-fit

lognormals applied to the lidar backscatter data at 2-km altitude intervals up to 12 km, for various latitude bands from the GLOBE Nov 1989 and May/June 1990 campaigns. The GLOBE '89 and GLOBE '90 altitude bins are 1 km and 500 m wide respectively. The center altitudes are listed. For those cases exhibiting departures from lognormality, e.g., multimode populations, a 10-percentile to 90-percentile range is included.

Comparisons of the β values obtained with the JPL airborne backscatter lidar during the GLOBE Pacific campaigns at various altitudes and latitude bands can be made with CO_2 laser backscatter data taken over the north Atlantic and equatorial Atlantic *[Vaughan, et al., 1995]* with the LATAS (laser true airspeed system) instrument measuring local aerosol backscatter (at 10.6 μm wavelength) at flight altitudes. *Vaughan et al. [1 995]* report results of measurements taken in the 1988-1990 period, 'I'hey grouped their observations into four altitude ranges: 0-3 km, 3-8 km, 8-12 km, and 12-16 km. Their median β values in the lowest range, containing the PBL, are consistent with our observations except for their Northeast Atlantic summer and winter values, which are much higher, about $2 \times 10^{-7} m^{-1} sr^{-1}$. We find a wide dynamic range of aerosol backscatter in the 3-8 km altitude region, with the lower altitudes heavily influenced by convective activity lifting aerosol' from below. In general their North Atlantic 3-8 km data (winter, spring, and summer) are somewhat similar to the GLOBE northern extratropical spring 1990 data, whereas their corresponding equatorial Atlantic (Ascension Island vicinity) data are similar to the GLOBE spring 1990 tropical data. *The Vaughan, et al. [1995]* North Atlantic data in the 8-12 km region cover a wide dynamic range, and it is difficult to separate statistically the relative frequencies of the higher backscatter observations due to either thin cirrus or to connectively lifted aerosol. The observed aerosol β values in the equatorial Atlantic are about a factor of 2 above those observed in the GLOBE spring 1990 tropical data and close to a factor of 5 above those of the GLOBE fall 1989 tropical data. Their 12-16 km data, excluding those which

are cjrrus-influenced, appear to result in β values which are within a factor of 2 of the GLOBE spring 1990 northern hemisphere data, There was very little statistically significant data above 12 km from GLOBE 1989, and the southern hemispheric GLOBE 1990 data were influenced by the Kelut aerosol in the 12-16 km region. It should be noted that the *Vaughan et al. [1995]* measurements were made at 10.6 μm, and that in general the β(9.25-μm)/β(10.6-μm) ratio for a baseline upper tropospheric aerosol population composed primarily of sulfuric acid is in the 2-4 range. Thus these comparisons lead to the conclusion that the aerosol mass in the Pacific mid- and upper-troposphere is less than that in the corresponding atmosphere above the Atlantic, but within an order of magnitude.

Comparison of our data with the data presented in *Rothermel et al. [1996]* is also useful. The *Rothermel et al.* [1996] data were taken during the GLOBE spring, 1990 campaign, primarily at the standard flight altitude range, 7.5-8.S km, at a wavelength of 9.1 μm. Their data were divided into northern and southern hemisphere categories. They observed a β mode in both hemispheres which peaked near $3 \times 10^{-11}\ m^{-1}\ sr^{-1}$; although it was the dominant SH mode, it was a smaller, secondary mode in the NH. The NH distribution contained a mode with a higher, sharper peak at $1.5 \times 10^{-10}\ m^{-1}\ sr^{-1}$. As can be seen in Figure 4 the larger backscatter mode is consistent with our lidar measurements north of 15° N. Our SH data at 7.5 km altitude are consistent with their lower β mode. It should be noted that based on our lidar observations there was less aerosol mass (lower number density of optically active aerosol) in the free troposphere above the Pacific during the GLOBE November, 1989 time period than the GLOBE May/June, 1990 time period.

4. CONCLUSIONS

The airborne lidar observations during the G] OBE fall, 1989 and spring, 1990 circumnavigations of the Pacific provided extensive latitude surveys of the tropospheric aerosol distributions during periods which included a range of aerosol source strengths. Putting these periods into temporal context, the stratosphere was in a near background aerosol condition during the fall, 1989 period, while the Kelut eruption of February, 1990 produced a significant aerosol source which migrated primarily into the southern hemisphere by the time of the GLOBE May/June, 1990 flight series. The scheduling of the two flight missions permitted observation of the springtime enhancements of tropospheric aerosol in the extratropical latitudes from surface sources.

The range of measured aerosol backscatter coefficients was found to be between three and four orders of magnitude in the free troposphere (from several times 10^{-12} m^{-1} sr^{-1} to slightly more than 10^{-8} m^{-1} sr^{-1}). The low values in the free troposphere, corresponding to baseline, or background aerosol conditions, are in agreement with Mie calculations based on previously published two-component lognormal fits to size distribution data as measured by on-board particle counters, assuming a sulfate aerosol in the 30-100 ng m^{-3} mass density range, with r_{eff} being 0,13-0.15 μm for the total distribution and in the range 0.20-0.28 μm for the larger particle mode only. The high values are in agreement with the assumption of an aerosol whose large particles are predominantly dust (refractory material), with size distributions measured by the particle counters during the relevant GLOBE flights, r_{eff} being in the range 0.85- 1,1 μm.

Elevated aerosol backscatter was observed in the upper troposphere at high northern and southern latitudes during their respective springtime periods. A local maximum appeared in the 8-10 km altitude range at high southern latitudes, poleward of 60° S. During these springtime periods the lower and middle tropospheric altitudes in this 60°-700 latitude range appeared to contain tenuous clouds of large extent, providing high backscatter with optical depths typically no more than a few tenths.

The lidar aerosol backscatter profiles clearly support the prior evidence of a much stronger springtime enhancement of aerosol mass in the northern hemisphere troposphere than in the southern hemisphere, the profiles providing evidence of the lifting of the surface-derived aerosol to altitudes as high as 12 km, reaching tropopause altitudes north of 40° N. These spatial-scale observations of springtime convection of surface-derived and PBL aerosol into the upper troposphere are in agreement with observations based on SAGE II zonal and seasonal average data [Kent et al., 1995]. The enhanced aerosol appears in distinct layers; the assumption of an aerosol mass which steadily declines with increasing altitude above the PBL, characterized by a scale height, is not accurate. Drawing from on-board *in situ* sensor data taken during passage through representative layers of this enhanced aerosol, it is determined that the lidar backscatter coefficients near or slightly above $10^{-8}\ m^{-1}sr^{-1}$ at the aerosol layer peaks are consistent with a dust mode of geometric mean radius 0. S-0.6 μm, s in the range 1.6-1.8, and No - 0. S-1 cm^{-3}, corresponding to a mass density near $3\ \mu g\ m^{-3}$. Using these size distribution characteristics and Mie scattering computations, the total optical depths through several examples of these layers have been found to be near 10^{-3} at the 9.25 μm lidar wavelength,

A sharp distinction was observed during both GLOBE missions between the aerosol backscatter characteristics of the tropical regions of intense convective activity, where there was very low mass density of aerosol particles in the lidar active size regime, and the subtropics. This is consistent with the contrast between the high wet deposition removal rates in the tropics vs. the relatively low removal rates in the dry subtropics. During the November, 1989 period an aerosol backscatter minimum appeared both in the PBL and free troposphere near 5°-10° N, with minimum free tropospheric aerosol backscatter in the 10° S to 20° N latitude range. During the May/June, 1990 period a well-defined transition occurred near 15° N, the prominent aerosol layers at the higher

latitudes rapidly disappearing south of this latitude. The latitude dependence of aerosol backscatter was dominated by the very large hemispheric asymmetry in aerosol source strength during this period.

The latitude surveys of PBL thickness and the strength of the PBL aerosol backscatter coefficient clearly indicate minima in the tropical latitudes where the cumulus convection activity is strong, maxima near the subtropical latitudes and high southern latitudes (near 60° S). The range of measured aerosol backscatter coefficients, which is governed by the surface wind speed and the relative humidity, spanned nearly two orders of magnitude in the PBL (just above $10^{-9}\ m^{-1}\ sr^{-1}$ to $10^{-7}\ m^{-1}\ sr^{-1}$). The magnitudes of the PBL aerosol backscatter coefficients at the 9.25 μm JPL lidar and 1,06 μm NASA Goddard Space Flight Center [*Spinhirne, et al.*, 1991] lidar wavelengths can be used in validation of the *Gathman [1983]* model, with modifications by *Gerber* [1991].

The penetration of the Kelut volcanic aerosol plume into the southern hemisphere troposphere was evident during the May/June 1990 mission. 'l'he lidar data indicate tongues of volcanic aerosol material crossing the tropopause at latitudes poleward of 20° S, influencing the aerosol content of the upper troposphere primarily in the subtropical and mid-latitudes.

Acknowledgements

The authors would like to acknowledge A. Brothers at JPL for contributions to data processing and display algorithms. Informative discussions with D. Bowdle, J. Rothermel, and V. Srivastava of NASA Marshall Space Flight Center, J. Spinhirne and S. Chudamani of NASA Goddard Space Flight Center, and G. Kent of Science and Technology Corp. have also been very helpful. This work was carried out by the Jet Propulsion laboratory, California Institute of Technology, under contract with the National Aeronautics and Space Administration,

REFERENCES

Balkanski, Y. J., D.J. Jacob, G.M. Gardner, W.C. Graustein, and K.K. Turekian, Transport and residence times of tropospheric aerosols inferred from a global three-dimensional simulation of ^{210}Pb, *J.Geophys. Res., 98, 20,573-20,586,* 1993.

Bodhaine, B.G., Mendonca, B. G., J.M. Harris, and J.M. Miller, Seasonal Variations in Aerosols and Atmospheric Transmission at Mauna Loa Observatory, *J. Geophys. Res., 86, 7395-7398,* 1981.

Bowdle, D. A., S.F. Williams, J. Rothermel, and J.E. Arnold, The GLObal Backscatter Experiment (GLOBE) Pacific Survey Mission, paper FA2-1, Topical Meeting on Coherent Laser Radar, Keystone, CO, July 8-12, 1991 (1991 Technical Digest Series, Volume 12, Optical Society of America, Washington, D.C.).

Brogniez, C., and L. Lenoble, Analysis of S-year data from the Stratospheric Aerosol and Gas Experiment **11,.7.** *Geophys. Res.,* 96, 15,479-15,497, 1991.

Brogniez, C., R. Santer, B.S. Diallo, M. Herman, and J. Lenoble, Comparative observations of stratospheric aerosols by ground-based lidar, balloon-borne polarimeter, and satellite solar occultation, *J. Geophys. Res.,* 97, 20,805-20,823, 1992.

Clarke, A. D., Atmospheric nuclei in the Pacific midtroposphere: their nature, concentration, and evolution, *J. Geophys. Res., 98, 20,633-20,647,* 1993.

Coakley, J. A., Jr., R. II, Cess, and F.B. Yurevich, The effect of tropospheric aerosols on the Earth's radiation budget: A parameterization for climate models", *J. Atmos. Sci., 40,* 116-138, *1983.*

Cutten, D. R., R.F. Pueschel, D.A. Bowdle, V. Srivastava, A.D. Clarke, J. Rothermel, J.D. Spinhirne, and R.T. Menzies, Multi-wavelength comparison of modeled and measured remote tropospheric aerosol backscatter over Pacific Ocean, *J. Geophys. Res., 101,* to be published, 1996.

Danielsen, E. F., Stratospheric-Tropospheric exchange based on radioactivity, ozone, and potential vorticity, *J. Atmos. Sci., 25, 502-518, 1968.*

Danielsen, E. F., and V.A. Mohnen, Project Duststorm report: Ozone transport, in situ measurements, and meteorological analyses of tropopause folding, *J. Geophys. Res., 82,* S867-5877, 1977.

Danielsen, E. F., R.S. Hipskind, S.E. Gaines, G.W. Sachse, G.],. Gregory, and G.F. hill, Three-dimensional analysis of potential vorticity associated with tropopause folds and observed variations of ozone and carbon monoxide, *J. Geophys. Res.,* 92,2103-2111, 1987.

Darzi, M., and J.W Winchester, Aerosol characteristics at Mauna Loa Observatory, Hawaii, after East Asian dust storm episodes, *J. Geophys. Res.,* **87, 1251-1258,** 1982.

Dutton, E. G., P, Reddy, S. Ryan, and J.J. DeLuisi, Features and effects of aerosol optical depth observed at Mauna Loa, Hawaii: 19$2-1992, .7. *Geophys. Res.*, 99, 8295-8306, 1994.

Gao, Y., R. Arimoto, M.Y. Zhou, J.T. Merrill, and R.A. Duce, Relationships between the dust concentrations over eastern Asia and the remote North Pacific, .7. *Geophys. Res.*, 97, 9867-9872, 1992.

Gathman, S. G., Optical properties of the marine aerosol as predicted by the navy aerosol model, *Opt. Eng., 22, 57-62, 1983.*

Gerber, H., Probability distribution of aerosol backscatter in the lower marine atmosphere at CO_2 wavelengths, *J. Geophys. Res.*, 96, 5307-5314, 1991,

Halpern, D. W. Knauss, O. Brown, and F. Wentz, An Atlas of Monthly Mean Distributions of SSMI Surface Wind speed, ARGOS Buoy Drift, AVHRR/2 Sea Surface Temperature, and ECMWF Surface Wind Components During 1990, JPL Publication 93-1, Jet Propulsion Laboratory, Pasadena, CA, 1993.

Haynes, P.]]., C.J. Marks, M.E. McIntyre, T.G. Shepherd, and K.P. Shine, On the "downward control" of extratropical diabatic circulations by eddy -included mean zonal forces, *J. Atmos. Sci., 48, 6S1-678, 1991.*

Hitchman, M. H., M, McKay, and C.R. Trepte, A climatology of stratospheric aerosol, *J. Geophys. Res.,* 99, 20,689-20,700, 1994.

1 Ioerling, M. P., T.K. Schaack, and A.J. Lenzen, A global analysis of stratospheric-tropospheric exchange during northern winter, *Mon. Wea. Rev., 121*, 162-172, 1993.

Hofmann, D. J., Twenty years of balloon-borne tropospheric aerosol measurements at Laramie, Wyoming, *J. Geophys. Res., 98*, **12,753-12,766,** 1993.

Holton, J. R., On the global exchange of mass between the stratosphere and troposphere, *J. Atmos. Sci.*, 47, 392-39S, 1990.

Kavaya, M.J., and R.T. Menzies, Lidar aerosol backscatter measurements: systematic, modeling, and calibration error considerations, *Appl. Opt., 24, 3444-3453, 1985.*

Kent, G. S., G.K. Yue, U.O. Farrukh, and A. Deepak, "Modeling atmospheric aerosol backscatter at CO_2 laser wavelengths, 1: Aerosol properties, modeling techniques, and associated problems", *Appl. Opt.*, 22, 1655-1665, 1983.

Kent, G. S., G.K. Yue, U.O. Farrukh, and A. Deepak, "Modeling atmospheric backscatter at CO_2 laser wavelengths. 2: Modeled values in the atmosphere", *Appl. Opt., 22, 1666-1670,* 1983.

Kent, G, S., D.M. Winker, M.T. Osborn, and K.M. Skeens, A Model for the Separation of Cloud and Aerosol in SAGE II occultation Data, *J. Geophys. Res., 98, 20,725-20,735, 1993.*

Kent, G. S., P.-H. Wang, M.P. McCormick, and K.M. Skeens, Multiyear Stratospheric Aerosol and Gas Experiment 11 measurements of upper tropospheric aerosol characteristics, *J. Geophys. Res., 100, 13,875-13,899, 1995,*

Kristament. 1. S., M.J. Harvey, and J. Il. Liley, A Seasonal Cycle in the Southwest Pacific Free Tropospheric Aerosol Concentration, *J. Geophys. Res., 98, 16,829-16,837,* 1993.

Kritz, M., S.W. Rosner, E. F'. Danielsen, and H.B. Selkirk, Air mass origins and troposphere-to-stratosphere exchange associated with mid-latitude cyclogenesis and tropopause folding inferred from ^{7}Be measurements, *J. Geophys. Res.,* 96, 17,405-17,414, 1991.

Lacis, A., J. Hansen, and M. Sate, "Climate forcing by stratospheric aerosols", *Geophys. Res. Lett., 19*, 1607-1610, 1992.

Lambert, G., J. Sanak, and G. Polian, Mean residence time of the submicrometer aerosols in the global troposphere, in Precipitation Scavenging, Dry Deposition, and Resuspension, vol. *2,* edited by H. R. Pruppacher, R. G. Semonin, and W, G. N. Slinn, pp. 1353-1359, Elsevier, New York, 1983.

Menzies, R. T., G.M. Ancellet, D.M. Tratt, M.G. Wurtele, J.C. Wright, and W. Pi, Altitude and seasonal characteristics of aerosol backscatter at thermal IR wavelengths using lidar observations from coastal California, *J. Geophys. Res.,* 94, 9897.9908, 1989.

Menzies, R.T., and D.M. Tratt, Airborne CO_2 coherent lidar for measurements of atmospheric aerosol and cloud backscatter, *Appl. Opt., 33, 5698-5711,* 1994.

Menzies, R. T., and D.M. Tratt, Evidence of seasonally dependent stratosphere-troposphere exchange and purging of lower stratospheric aerosol from a multiyear lidar data set, *J. Geophys. Res., 100,* 3139-3148, 1995.

Palmer, K. F., and D. Williams, Optical constants of sulfuric acid: applications to the clouds of Venus?, *Appl. Opt., 14,* **208-219,** 1975.

Barrington, J. R., W. H. 7.oiler, and N.K. Aras, Asian dust: Seasonal transport to the Hawaiian Islands, Science, 220, 195-197, 1983.

Parungo, F., Z. Li, X. Li, D. Yang, and J. Harris, Gobi dust storms and The Great Green Wall, *Geophys. Res. Lett.,* **21, 999-1002, 1994.**

Porter, J. N., A.D. Clarke, G. Ferry, anti R.F. Pueschel, Aircraft studies of size-dependent aerosol sampling through inlets, *J. Geophys. Res., 97, 3815-3824,* 1992.

Post, M. J., "Aerosol Backscattering Profiles at CO_2 Wavelengths: the NOAA Data Base", *Appl. Opt.,* 23, "2507-2509, 1984.

Post, M. J., Atmospheric purging of El Chichon debris, *J. Geophys. Res., 91,* 5222-5228, 1986.

Post, M. J., and R.E. Cupp, "CO_2 lidar backscatter profiles over Hawaii during Fall 1988", *Appl. Opt., 31, 4590-4599,* 1992.

Pueschel, R. F., J.M. Livingston, G.V. Ferry, and T.E. DeFelice, Aerosol Abundances and Optical Characteristics in the Pacific Basin Free Troposphere, *Atmos. Environ., 28, 951-960, 1994.*

Randall, D. A., J.A. Abe]es, and T.G. Corsetti, Seasonal Simulations of the Planetary Boundary Layer and Boundary-Layer Stratocumulus clouds with a General Circulation Model, *J. Atmos. Sci., 42, 641-676, 1985.*

Rehfeld, S., and M. Heimann, Three dimensional atmospheric transport simulation of the radioactive tracers ^{210}Pb, ^{7}Be, ^{10}Be, and ^{90}Sr, *J. Geophys. Res., 100,* 26,141-26,161, 1995.

Reiter, E. R., Stratospheric-tropospheric exchange processes, *Rev. Geophys. Space Phys., 13, 459-474, 1975.*

Rosenlof, K. H., and J.R. Holton, Estimates of the stratospheric residual circulation using the downward control principle, *J. Geophys. Res., 98, 10,465-10,479, 1993.*

Rothermel, J., D.A. Bowdle, and V. Srivastava, Mid-tropospheric aerosol backscatter background mode over the Pacific ocean at 9.1 μm wavelength, *Geophys. Res. Lett., 23, 281-284, 1996.*

Rothermel, J., D.M. Chambers, M.A. Jarzembski, V. Srivastava, D.A. Bowdle, and W.D. Jones, Signal processing and calibration of continuous-wave focused CO_2 Doppler lidars for atmospheric backscatter measurement, *Appl. Optics,* to republished, 1996.

Russell, P.B., T.J. Swissler, and M.P. McCormick, Methodology for error analysis and simulation of lidar aerosol measurements, *Appl. Optics, 16', 3783-3797,* 1979.

Russell, P. B., E.F. Danielsen, R.A. Craig, and H.B. Selkirk, The NASA Spring 1984 Stratosphere-Troposphere Exchange Experiment: science objectives and operations, *J. Geophys. Res.,* 96, 17,401-17,404, 1991.

Sassen, K., Evidence for liquid-phase cirrus cloud formation from volcanic aerosols: climatic implications, *Science,* 2.$7, 516-519, 1992.

Shapiro, M. A., Turbulent mixing within tropopause folds as a mechanism for the exchange of chemical constituents between the stratosphere and troposphere, *J. Atmos. Sci.,* .?7, 994-1004, 1980.

Sheridan, P, J., C.A. Brock, and J.C. Wilson, Aerosol particles in the upper troposphere and lower stratosphere: Elemental composition and morphology of individual particles in northern midlatitudes, *Geophys. Res. Lett., 21,* 2587-2590, 1994.

Spinhirne, J. D., S. Chudamani, and J.F. Cavanaugh, Visible and near IR lidar backscatter observations on the GLOBE Pacific survey missions, in *Proceedings of the Seventh Symposium on Meteorological Observations and instrumentation with Special*

Sessions on Laser Atmospheric Studies (American Meteorological society, Boston, Mass., 1991) p. J261-J265.

Srivastava, V., M.A. Jarzembski, and D.A. Bowdle, Comparison of calculated aerosol backscatter at 9.1- and 2.1-μm wavelengths, *Appl. Opt., 31*, 1904-1906, 1992.

Srivastava, V., D.A. Bowdle, M.A. Jarzembski, J. Rothermel, D.M. Chambers, and D.R. Cutten, High resolution remote sensing of sulfate aerosols from CO_2 lidar backscatter, *Geophys. Res. Lett.,* 22,2373-2376, 1995.

Staley, D. O., On the mechanism of mass and radioactivity transport from stratosphere to troposphere, *J. Atmos. Sci., 19, 450-467, 1962.*

Thomason, L. W., A diagnostic stratospheric aerosol size distribution inferred from SAGE 11 measurements, *J. Geophys. Res.,* 96, 22,501-22,508, 1991.

Trepte, C. R., R.E. Veiga, and M.P. McCormick, The Poleward Dispersal of mount Pinatubo Volcanic Aerosol, *J. Geophys. Res., 98, 18,563-18,573,* 1993.

Tratt, D. M., and R.T. Menzies, Recent climatological trends in atmospheric aerosol backscatter derived from the Jet Propulsion laboratory multiyear backscatter profile database, *Appl. Opt.,* .33, 424-430, 1994.

Tratt, D. M., and R.T. Menzies, Evolution of the Pinatubo volcanic aerosol column above Pasadena, California observed with a mid-infrared backscatter lidar, *Geophys. Res. Lett.,* 22, 807-810, 1995.

Trepte, C. R., R.E. Veiga, and M.P. McCormick, The poleward dispersal of Mount Pinatubo volcanic aerosol, *J. Geophys. Res.,* 98, 18,563-18,573, 1993.

Uematsu, M., R.A. Duce, J.M. Prospero, L. Chen, J.T. Merrill, and R.]... McDonald, Transport of mineral aerosol from Asia over the North Pacific Ocean, *J. Geophys. Res., 88,* 5343-5352, 1983.

Vaughan, J. M., D.W. Brown, C. Nash, S.B. Alejandro, and G.G. Koenig, Atlantic atmospheric aerosol studies 2. Compendium of airborne backscatter measurements at 10.6 μm, .7. *Geophys. Res., 100,* 1043-1065, 199S.

World Meteorological Organization (WMO), Stratosphere-Troposphere Exchange, Chapter 5, in *Atmospheric Ozone: 1985* (Global Ozone Research and Monitoring }'reject, Report 16), pp. 151-240, Geneva, 1985.

Yamato, M., and H. Tanaka, Aircraft observations of aerosols in the free marine troposphere over the North Pacific ocean: Particle chemistry in relation to air mass origin, *J. Geophys. Res.,* 99, 5353-5377, 1994.

Table 1. Lognormal Parameters for Aerosol Backscatter Distributions Observed by Airborne Lidar during GLOBE '89

latitude	Altitude (km)	β_m (m^{-1} sr^{-1})	s
20 S-60S	*2.5*	1.2×10^{-10}	*3.7*
	4.5	$5.3X\ 10^{-11}$	2.7
	6.5	$3.1X\ 10^{-11}$	4.0
	8.5	$2.5x\ 10^{-11}$	6.2
	10.5	$2,6x\ 10^{-11}$	5.1
20 S - 20 N	2.s	$2.1X\ 10^{-10}$	3.3
	4.5	$3.4x\ 10^{-11}$	4.1
	6.5	$1.2X\ 10^{-11}$	3.2
	8.5	1.1×10^{-11}	3.8
	10.5	$7.3X\ 10^{-12}$	3.0
20 N-60N	2.5	3.1×10^{-10}	2.8
	4.5	$1.5X\ 10^{-10}$	5.0
	6.5	$8.7x\ 10^{-11}$	4.5
	8.25	$8.5X\ 10^{-12}$	3.6

Asterisks denote cases for which 20- and 80-percentiles are given.

Table 2. Lognormal Parameters for Aerosol Backscatter Distributions Observed by Airborne Lidar during GLOBE '90

Latitude	Altitude (km)	β_m (m^{-1} sr^{-1})	s
20 S-60S	2.25	*2.3X* 10^{-10}	*3.6*
	4,25	*2.8x* 10^{-11}	*3.4*
	6,25	*1.2X* 10^{-11}	*2.8*
	8.25	1.5 x 10^{-11}	3.1
	10.25	1.1 *x* 10^{-11}	*2.8*
20 S - 20 N	*2,25*	9.1 *x* 10^{-10}	*2.6*
	*4.25**	*1.7X* 10^{-10}	3(-11) to 1(-9)
	6.25*	3.9 x 10^{-11}	1(-11) to 3(-10)
	8,25	*3.2x* 10^{-11}	**2.8**
	10.25	2.0 x 10^{-11}	3.3
20 N-60N	*2.25*	3.1 *x* 10^{-9}	3.0
	4.2S	*8.5X* 10^{-10}	3.0
	*6.25**	3.1 x 10^{-10}	S(-11) to 2(-9)
	*8.25**	1.2 *x* 10^{-10}	2(-11) to 1.5(-9)
	10.25"	*4.2x* 10^{-11}	1(-11) to 3(-10)

Asterisks denote cases for which 20-and 80-percentiles are given.

FIGURE CAPTIONS

Figure 1. Flight tracks for the GLOBE airborne field campaigns over the Pacific, beginning and ending at Moffett Field, Mountain View, California,

Figure 2. Gaussian cumulative probability distribution of aerosol backscatter coefficients at 600 m altitude measured during the May 24, 1990 flight from Tahiti to Christchurch, New Zealand.

Figure 3. Aerosol backscatter coefficient as a function of latitude and altitude above the Pacific Ocean, at the 9.25 μm lidar wavelength, during the GLOBE November, 1989 flight series.

Figure 4. Aerosol backscatter coefficient as a function of latitude and altitude above the Pacific Ocean, at the 9.25 μm lidar wavelength, during the GLOBE May/June, 1990 flight series.

Figure 5. Aerosol backscatter coefficient as a function of longitude and altitude in the northern mid-latitude belt, at the 9.25 μm lidar wavelength, during the GLOBE May/June, 1990 flight series.

Figure 6. Aerosol backscatter profiles at the 9.25 μm lidar wavelength taken during the May 20, 1990 flight from Hawaii to American Samoa, The solid curve corresponds to observations at 14°N latitude, and the dashed curve corresponds to observations at 10.5° N latitude. (The dotted curve is the lidar noise-equivalent backscatter coefficient as a function of altitude.)

Figure 7. Aerosol backscatter profiles at the 9.25μm lidar wavelength taken during the May 31, 1990 flight from Darwin, Australia to Tokyo, Japan, The dashed curve corresponds to observations in the 12°-140 N latitude region, and the solid curve corresponds to observations in the 15°-160 N region.

Figure 8. Profiles of geometric mean aerosol backscatter coefficient vs. altitude for GLOBE May/June, 1990 observations. The data are grouped into three latitude bands: tropical (20° S to 20° N), southern hemisphere extratropical, and northern hemisphere extratropical. (See text for a discussion of the bifurcation of the tropical profile.)

Figure 9. Profiles of geometric mean aerosol backscatter coefficient vs. altitude for the tropical latitude band, comparing GLOBE November, 1989 observations with GLOBE May/June, 1990 observations.

Figure 10. Gaussian cumulative probability distribution of aerosol backscatter coefficients centered at 250 m altitude for the tropical latitude band, measured during the May/June, 1990 flights.

Figure 11. Gaussian cumulative probability distribution of aerosol backscatter coefficients centered at 250 m altitude for the 0-10° N band of the Hawaii to American Samoa flight and the 5° S to 20° N band of the Darwin to Tokyo flight during the May/June, 1990 flight series.

Figure 12. Gaussian cumulative probability distribution of aerosol backscatter coefficients centered at 250 m altitude for the remainder of the 20° S to 20° Nband during the May/June, 1990 flight series.

Figure 13. Gaussian cumulative probability distribution of aerosol backscatter coefficients centered at 250 m altitude for the northern extratropical latitude band during the May/June, 1990 flight series.

Figure 14. Gaussian cumulative probability distribution of aerosol backscatter coefficients centered at 250 m altitude for the southern extratropical latitude band during the May/June, 1990 flight series.

Figure 15. Surface wind speeds derived from the SSMI satellite sensor, for a fixed longitude slice in the western Pacific.

Figure 16. Gaussian cumulative probability distribution of aerosol backscatter coefficients centered at 5250 m altitude in the mid-troposphere, for the northern extratropical (20° - 60° N) latitude band.

GLOBE SURVEY MISSION FLIGHT TRACKS

GLOBE I

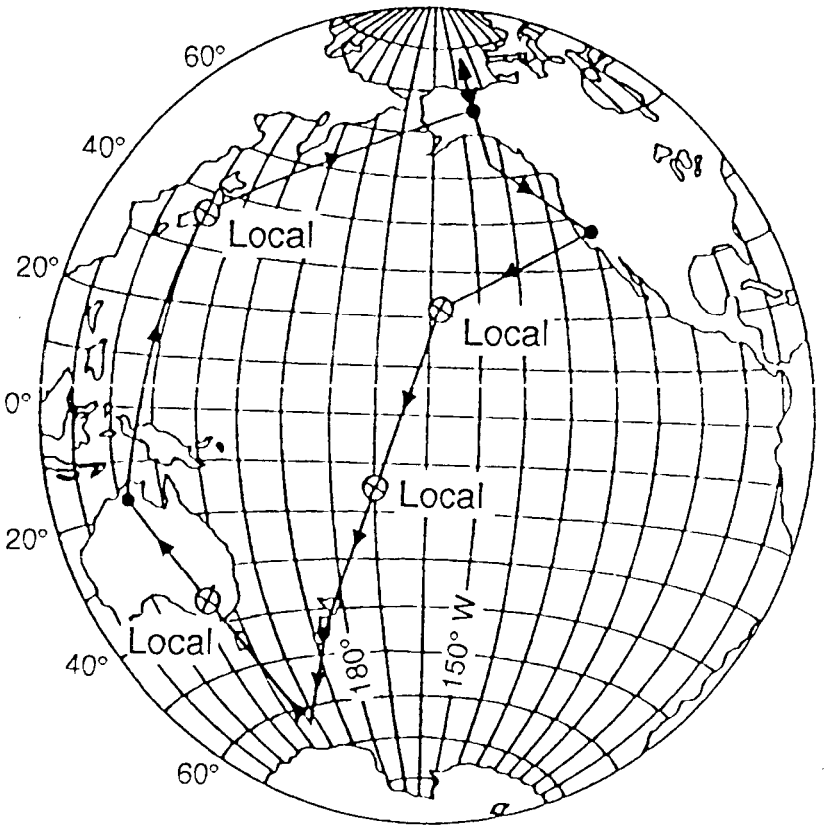

Fall 1989

GLOBE II

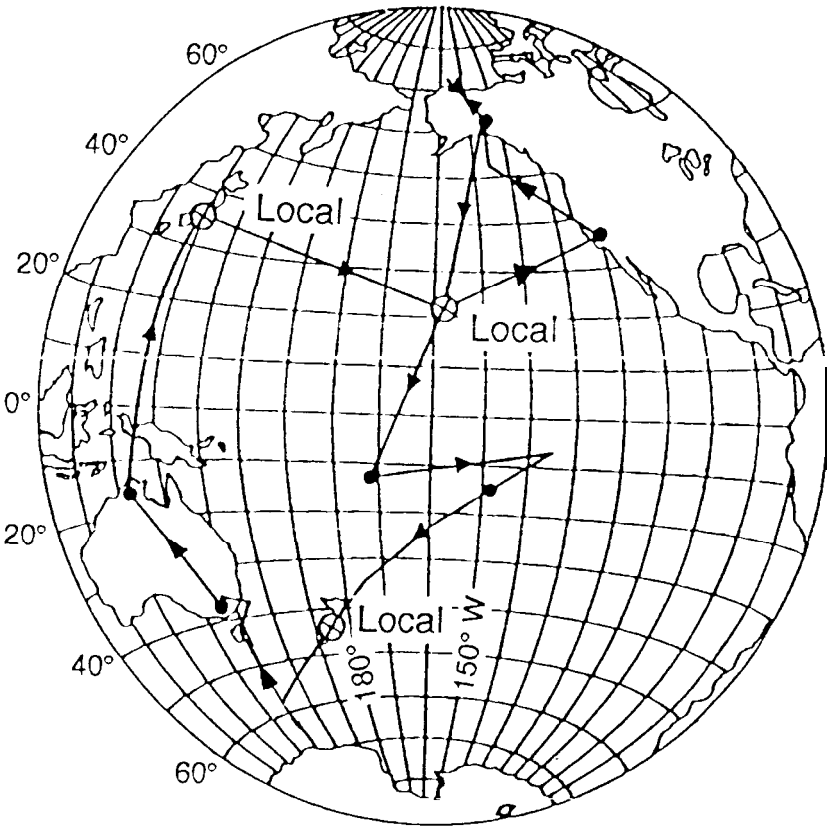

Spring 1990

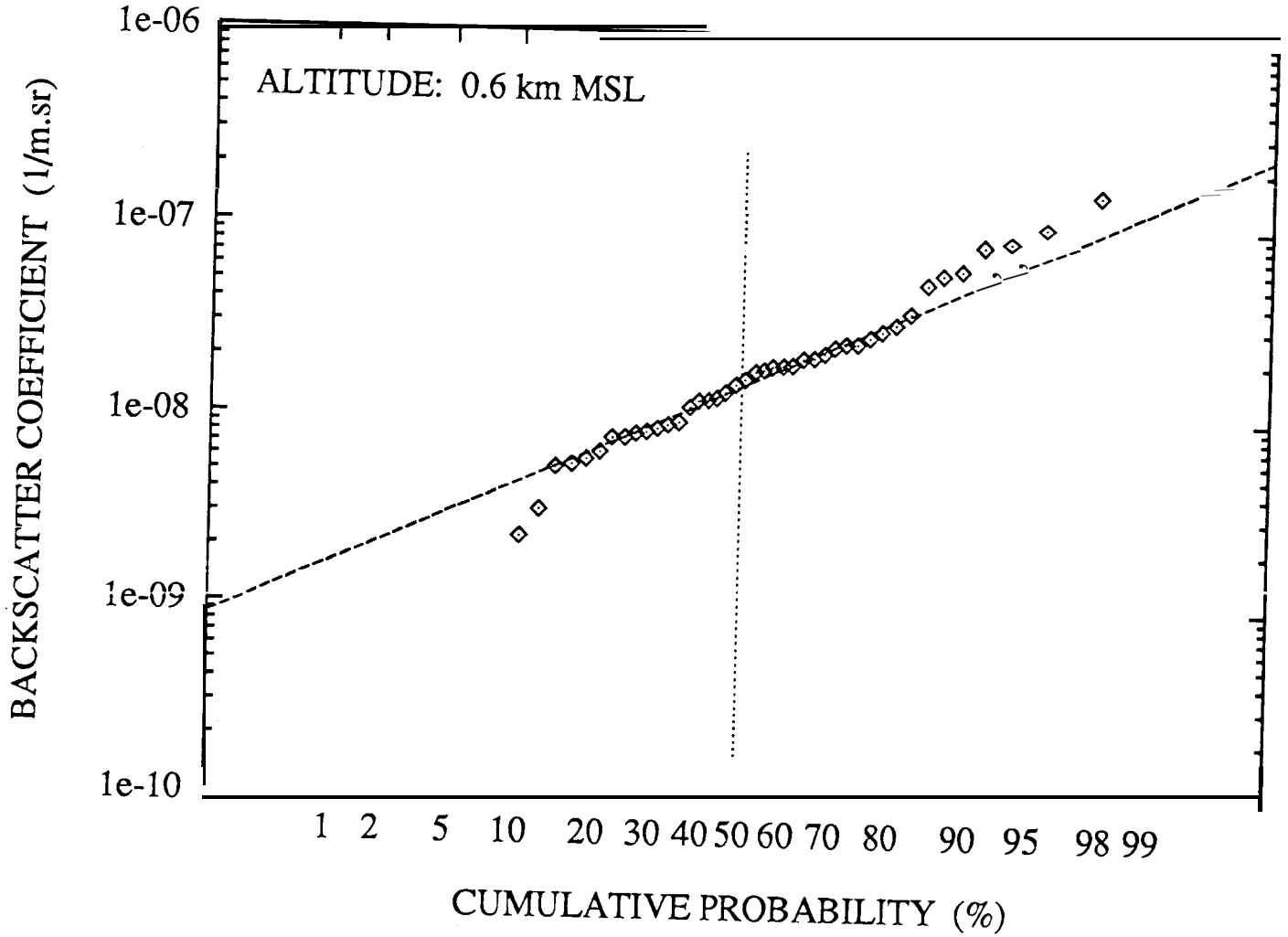
ALTITUDE: 0.6 km MSL
BACKSCATTER COEFFICIENT (1/m.sr)
1e-06
1e-07
1e-08
1e-09
1e-10
1 2 5 10 20 30 40 50 60 70 80 90 95 98 99
CUMULATIVE PROBABILITY (%)

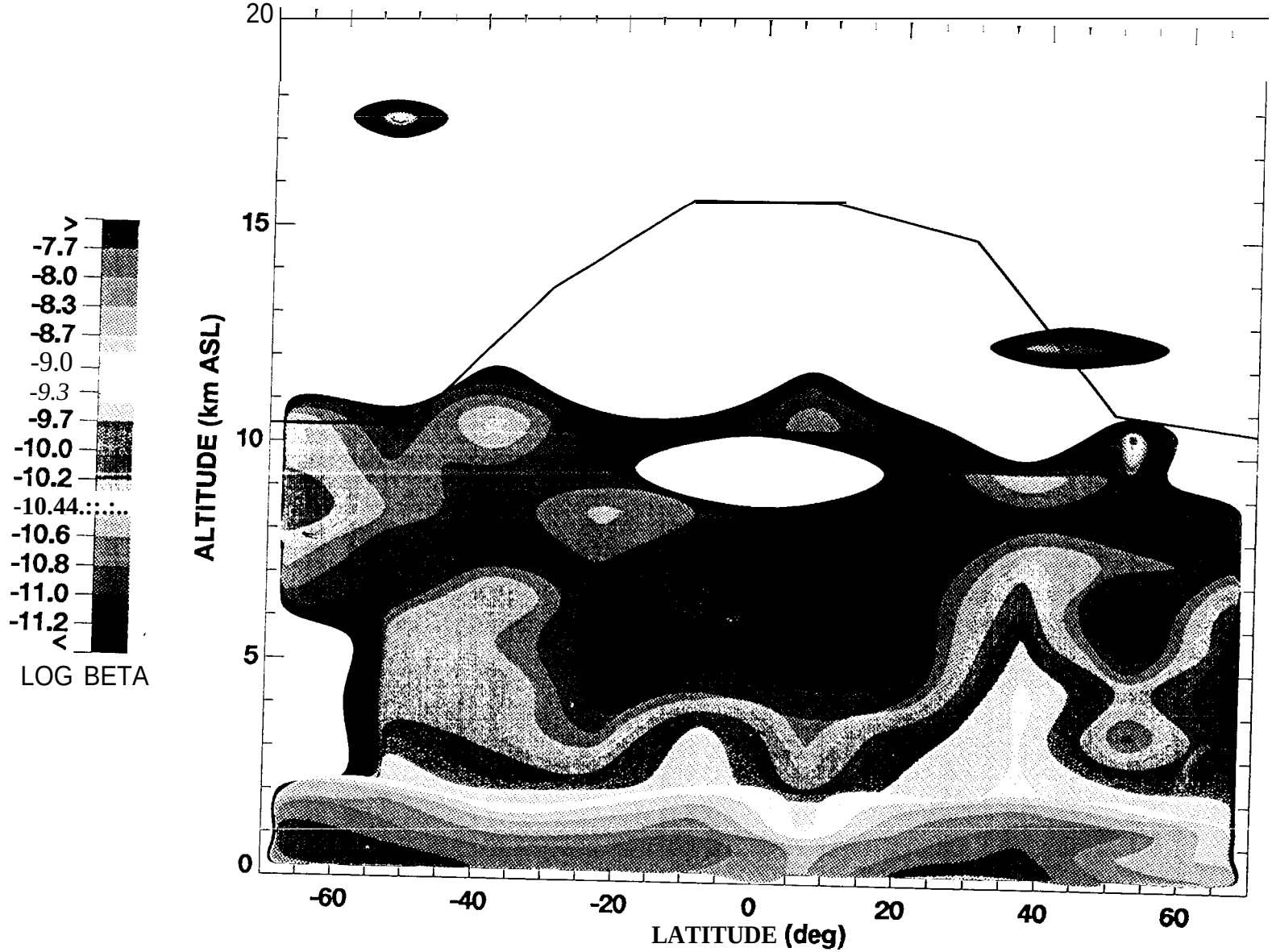
>
-7.7
-8.0
-8.3
-8.7
-9.0
-9.3
-9.7
-10.0
-10.2
-10.44
-10.6
-10.8
-11.0
-11.2
<
LOG BETA
20
15
10
5
0
ALTITUDE (km ASL)
-60
-40
-20
0
20
40
60
LATITUDE (deg)

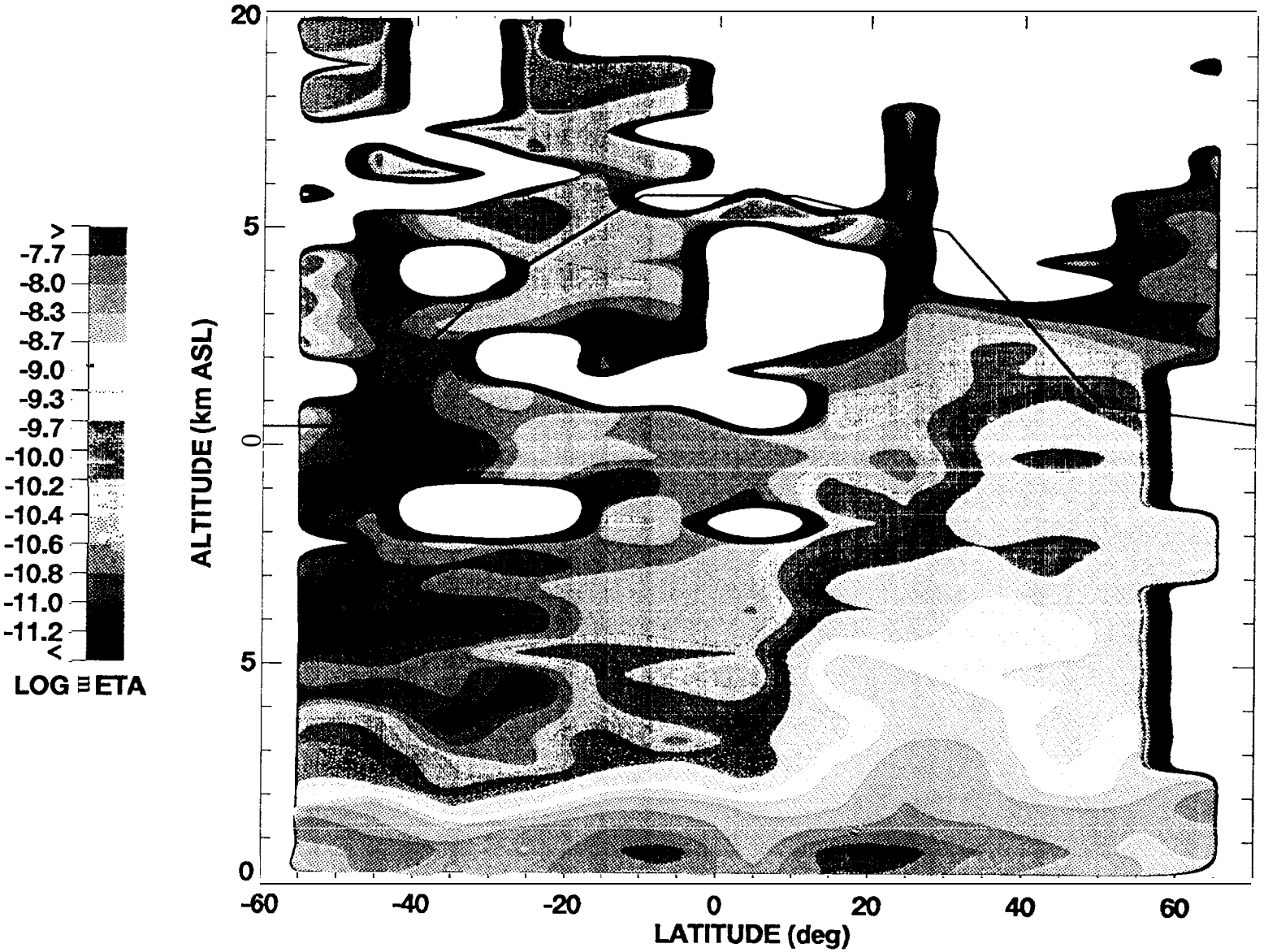
>
-7.7
-8.0
-8.3
-8.7
-9.0
-9.3
-9.7
-10.0
-10.2
-10.4
-10.6
-10.8
-11.0
-11.2
<
LOG ETA
ALTITUDE (km ASL)
20
5
0
5
0
-60
-40
-20
0
20
40
60
LATITUDE (deg)

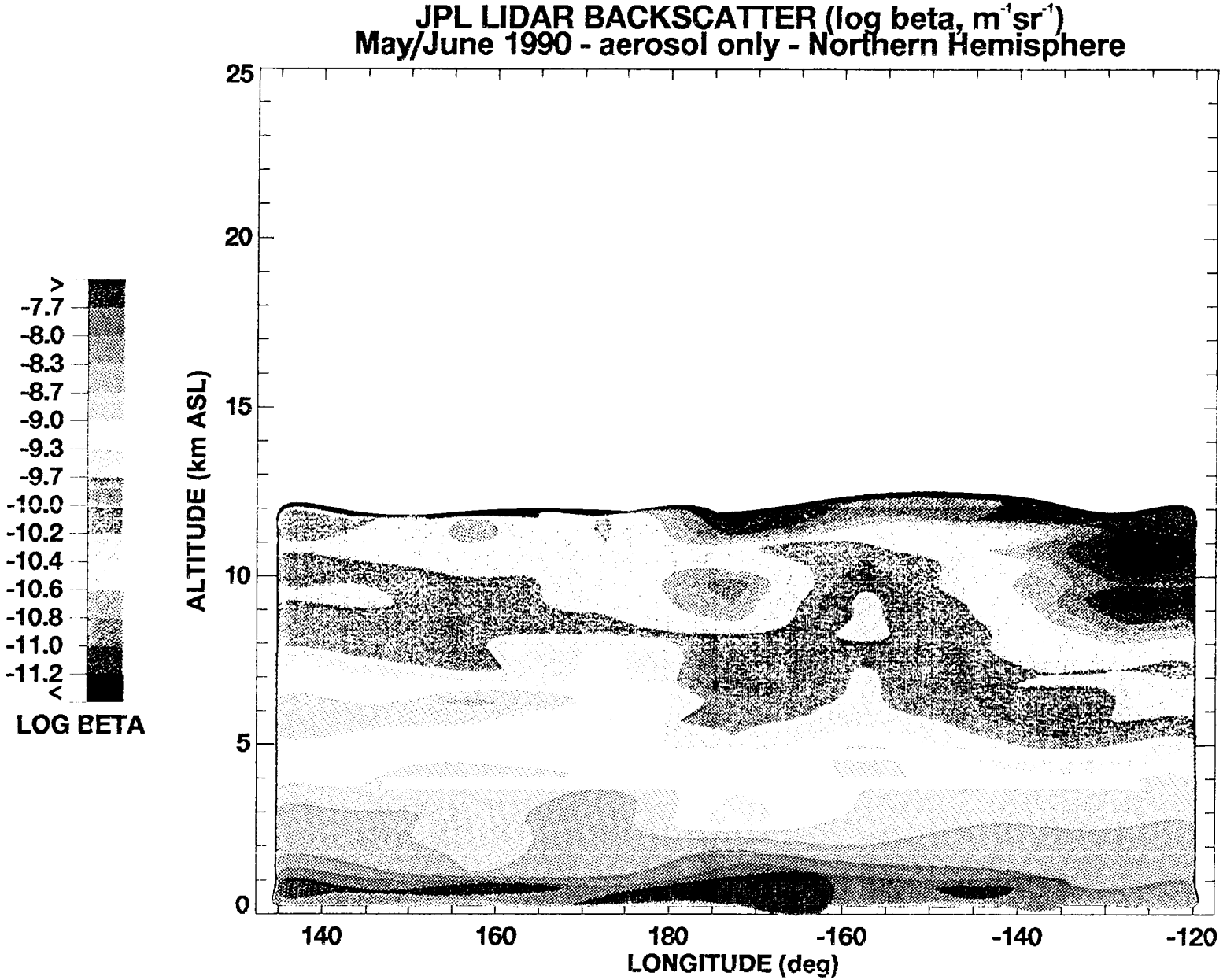
JPL LIDAR BACKSCATTER (log beta, m-1sr-1)
May/June 1990 - aerosol only - Northern Hemisphere
LOG BETA
> -7.7
-8.0
-8.3
-8.7
-9.0
-9.3
-9.7
-10.0
-10.2
-10.4
-10.6
-10.8
-11.0
-11.2
< -11.2
ALTITUDE (km ASL)
25
20
15
10
5
0
140
160
180
-160
-140
-120
LONGITUDE (deg)

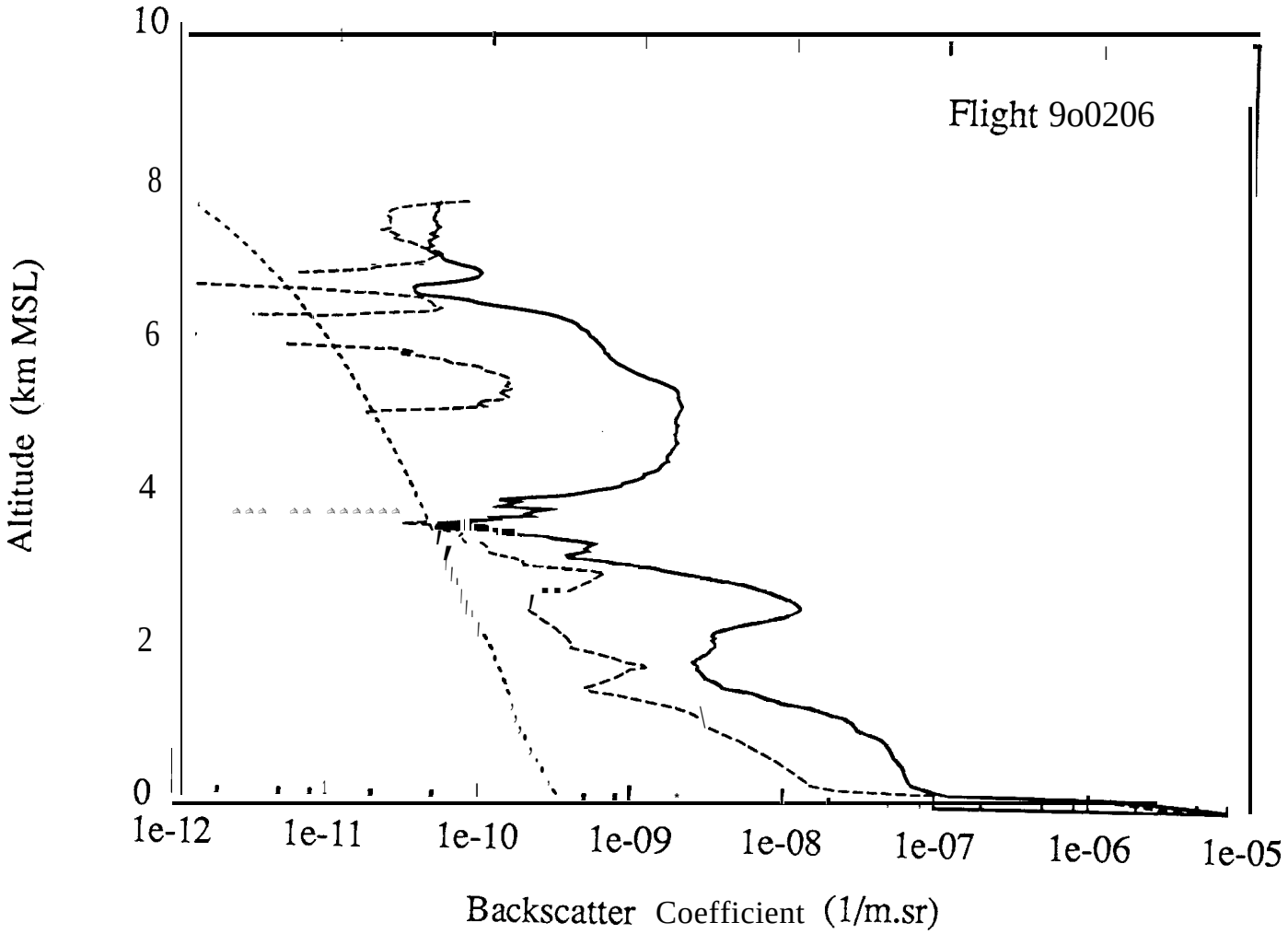
Flight 9o0206
Altitude (km MSL)
10
8
6
4
2
0
1e-12
1e-11
1e-10
1e-09
1e-08
1e-07
1e-06
1e-05
Backscatter Coefficient (1/m.sr)

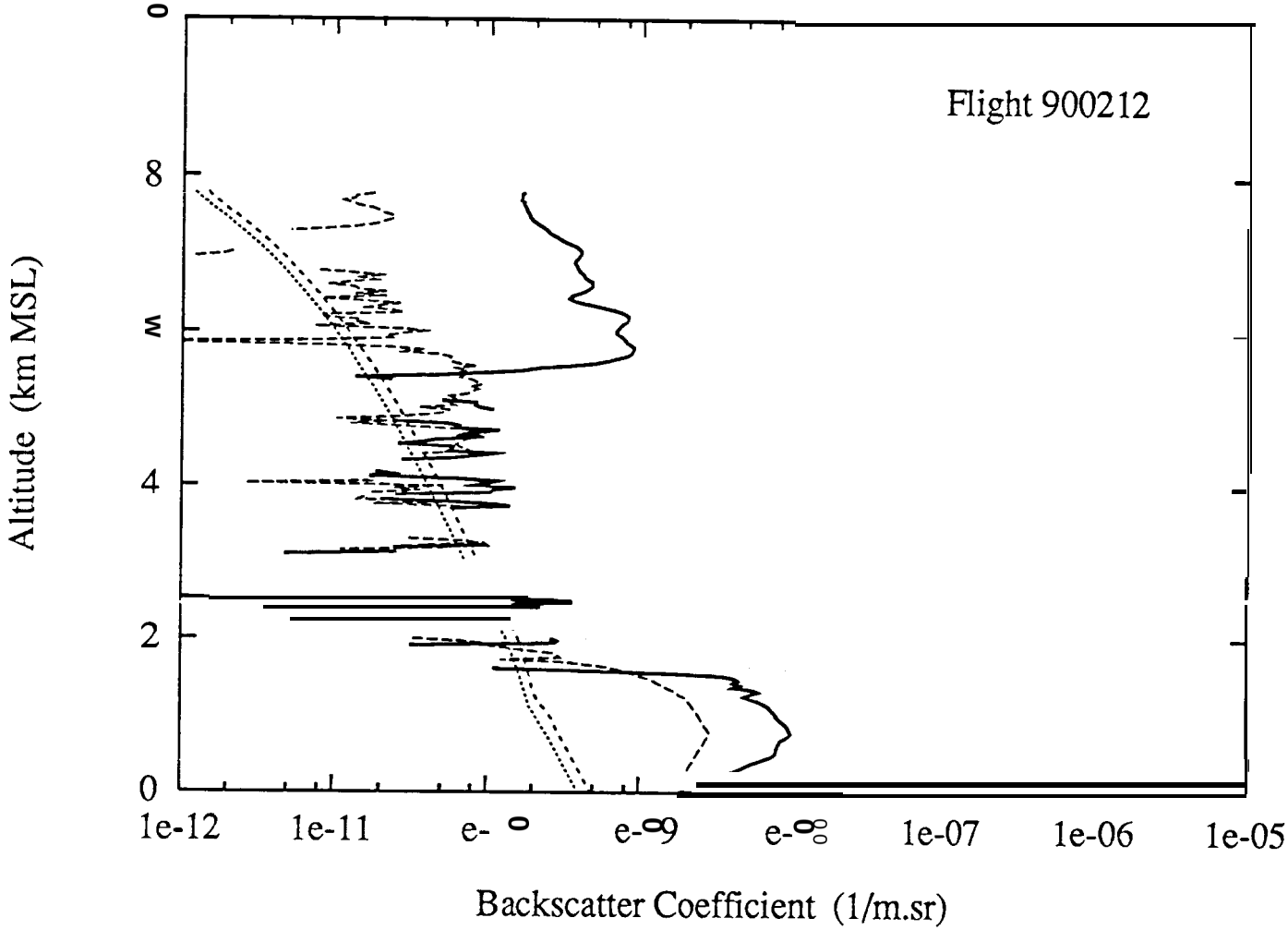
Flight 900212
Altitude (km MSL)
0
8
4
2
0
1e-12
1e-11
1e-07
1e-06
1e-05
Backscatter Coefficient (1/m.sr)

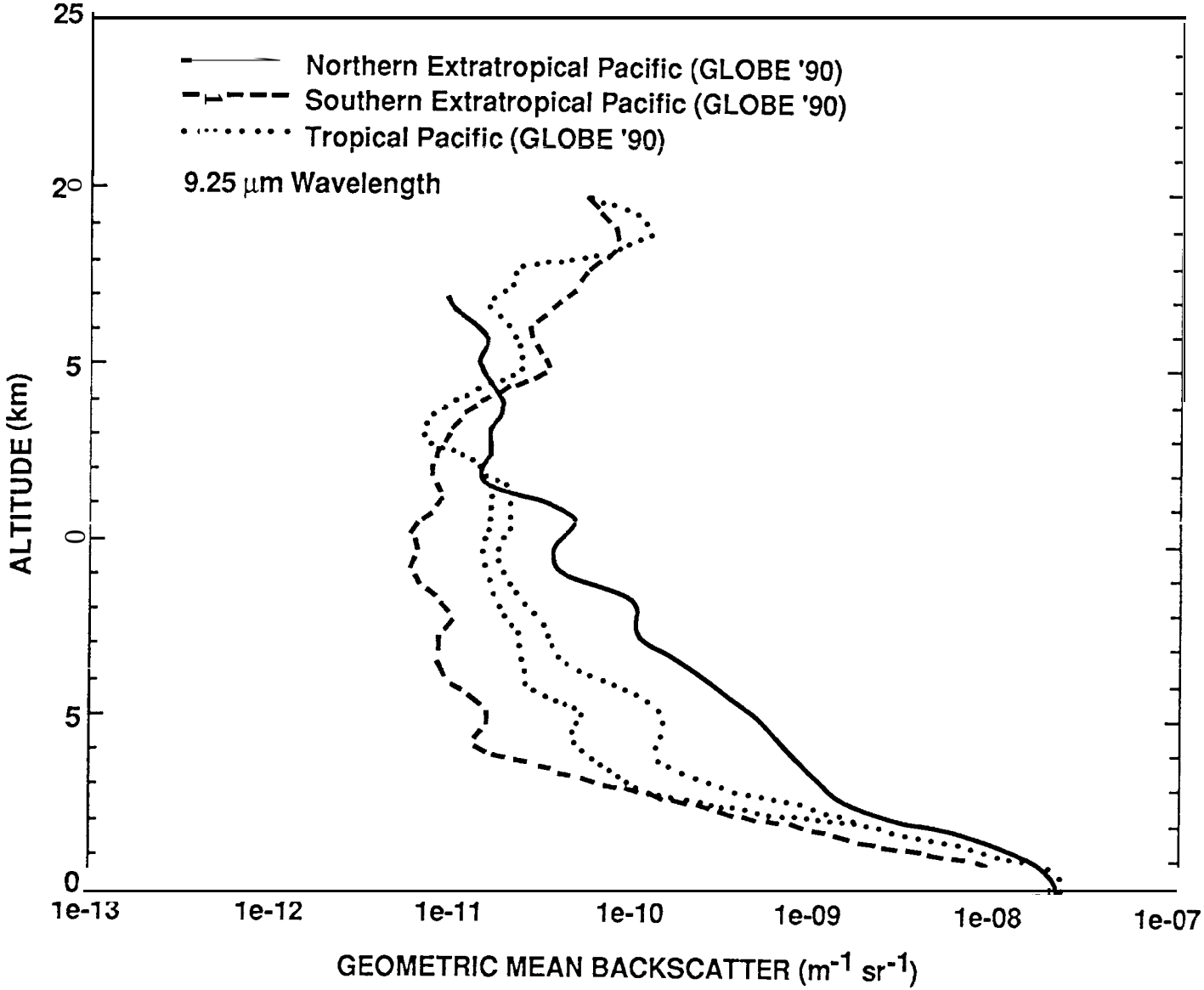
Northern Extratropical Pacific (GLOBE '90)
Southern Extratropical Pacific (GLOBE '90)
Tropical Pacific (GLOBE '90)
9.25 μm Wavelength
ALTITUDE (km)
25
20
5
0
5
0
1e-13
1e-12
1e-11
1e-10
1e-09
1e-08
1e-07
GEOMETRIC MEAN BACKSCATTER (m-1 sr-1)

Fig

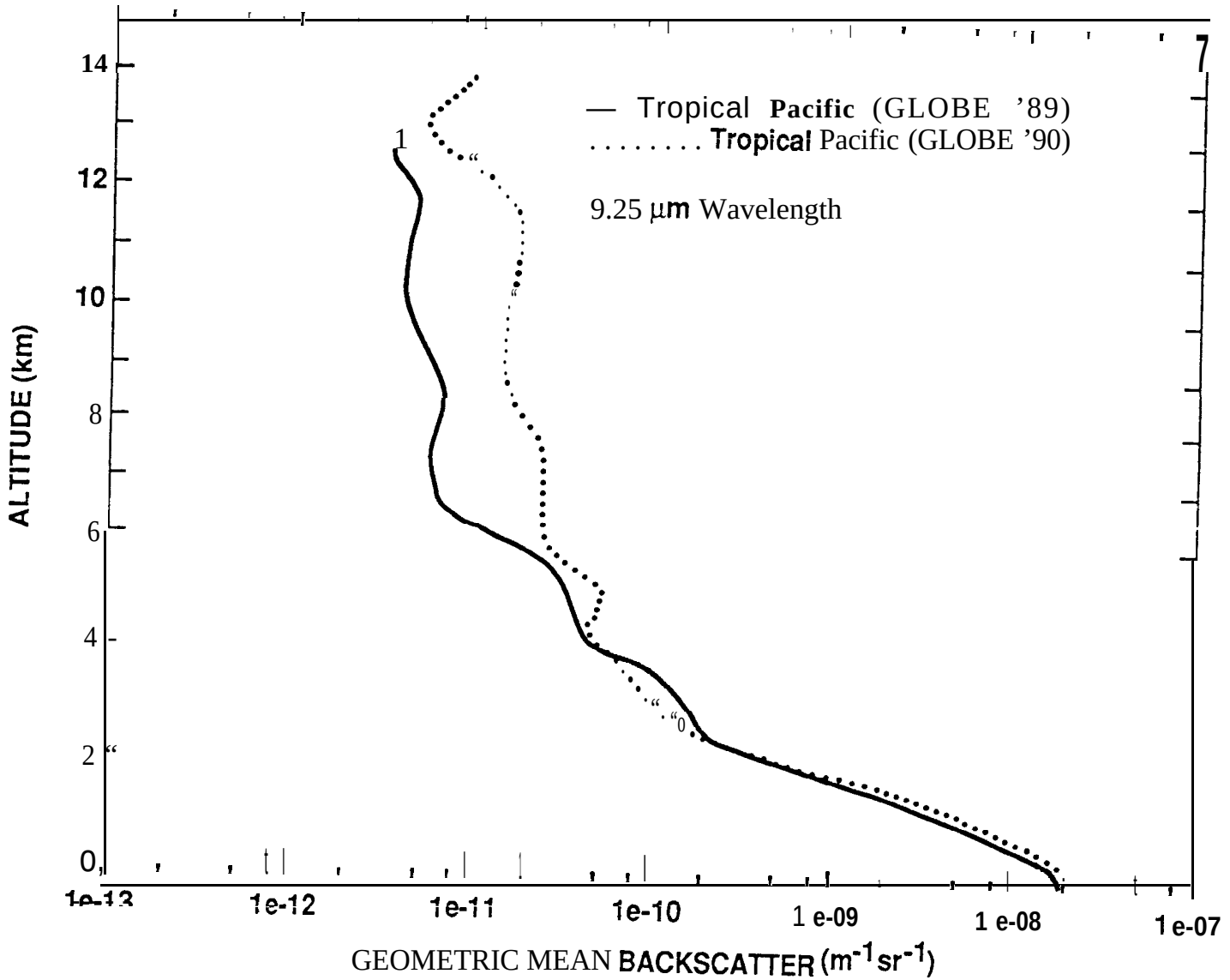
— Tropical Pacific (GLOBE '89)
..... Tropical Pacific (GLOBE '90)
9.25 μm Wavelength
ALTITUDE (km)
14
12
10
8
6
4
2
0
1e-13
1e-12
1e-11
1e-10
1 e-09
1 e-08
1 e-07
GEOMETRIC MEAN BACKSCATTER (m-1sr-1)

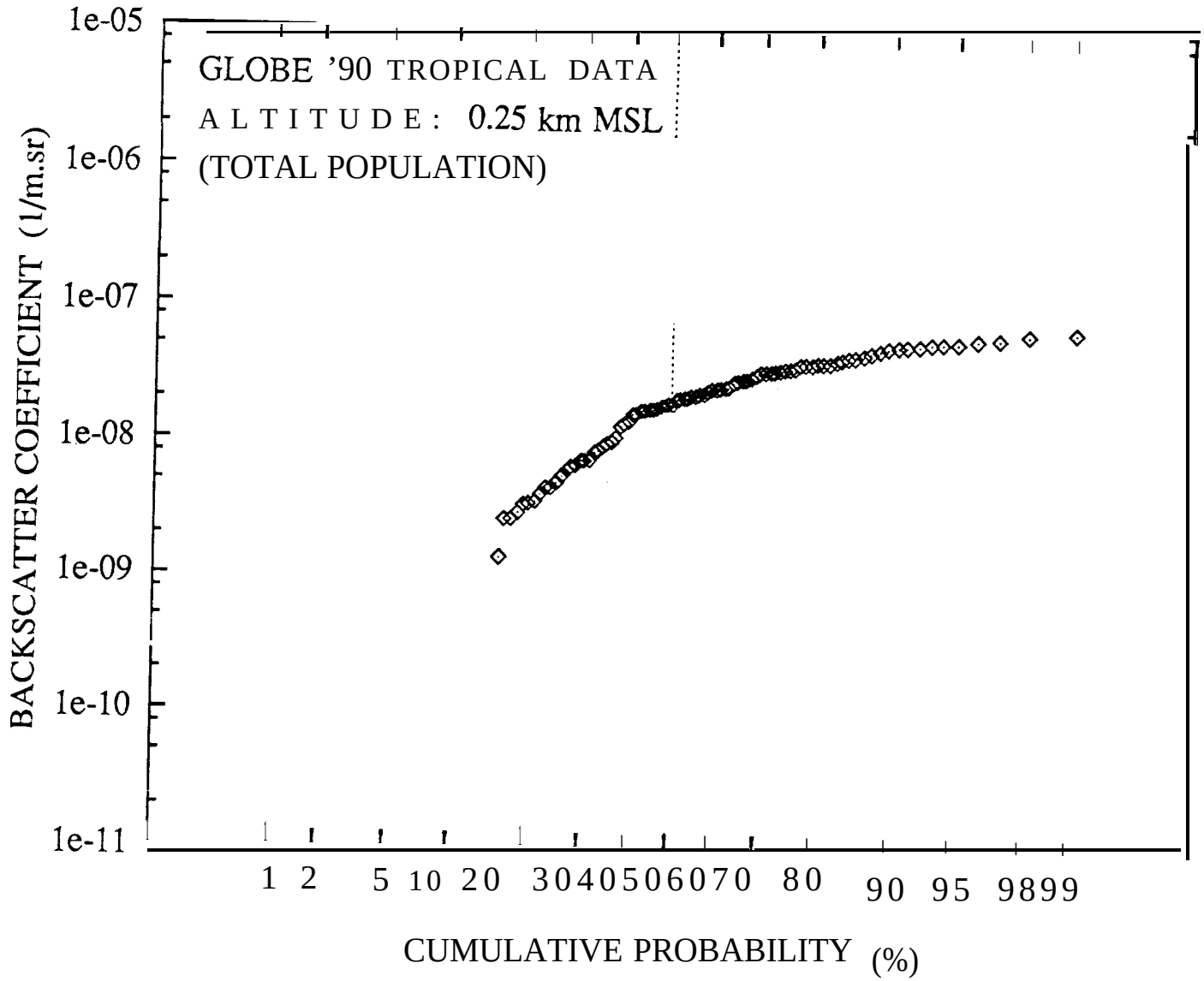
GLOBE '90 TROPICAL DATA
ALTITUDE: 0.25 km MSL
(TOTAL POPULATION)
BACKSCATTER COEFFICIENT (1/m.sr)
1e-05
1e-06
1e-07
1e-08
1e-09
1e-10
1e-11
1 2 5 10 20 30 40 50 60 70 80 90 95 98 99
CUMULATIVE PROBABILITY (%)

3/14/90

GLOBE '90: TROPICAL DATA (900212 and 9OO2O6[O-1ON] only)

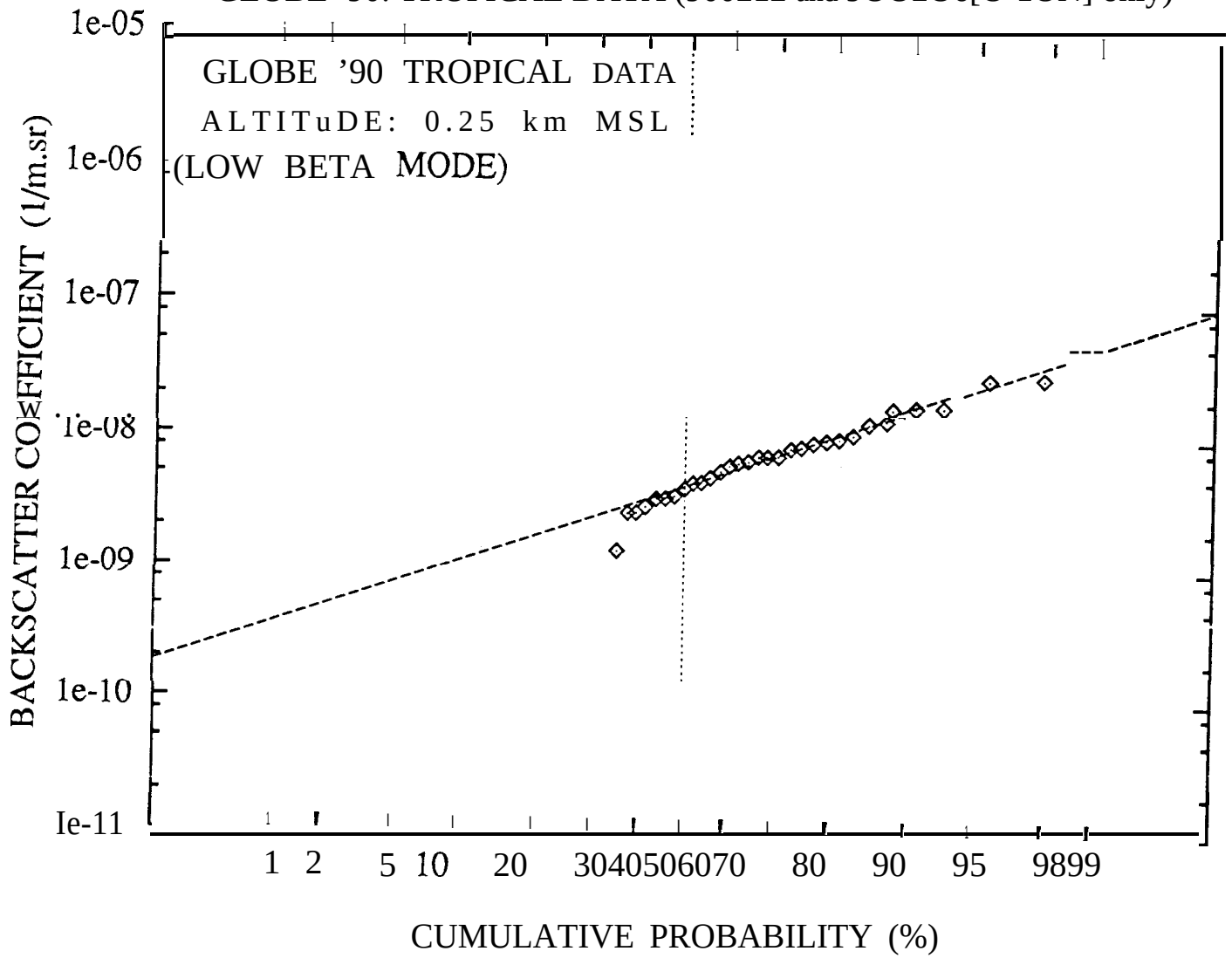

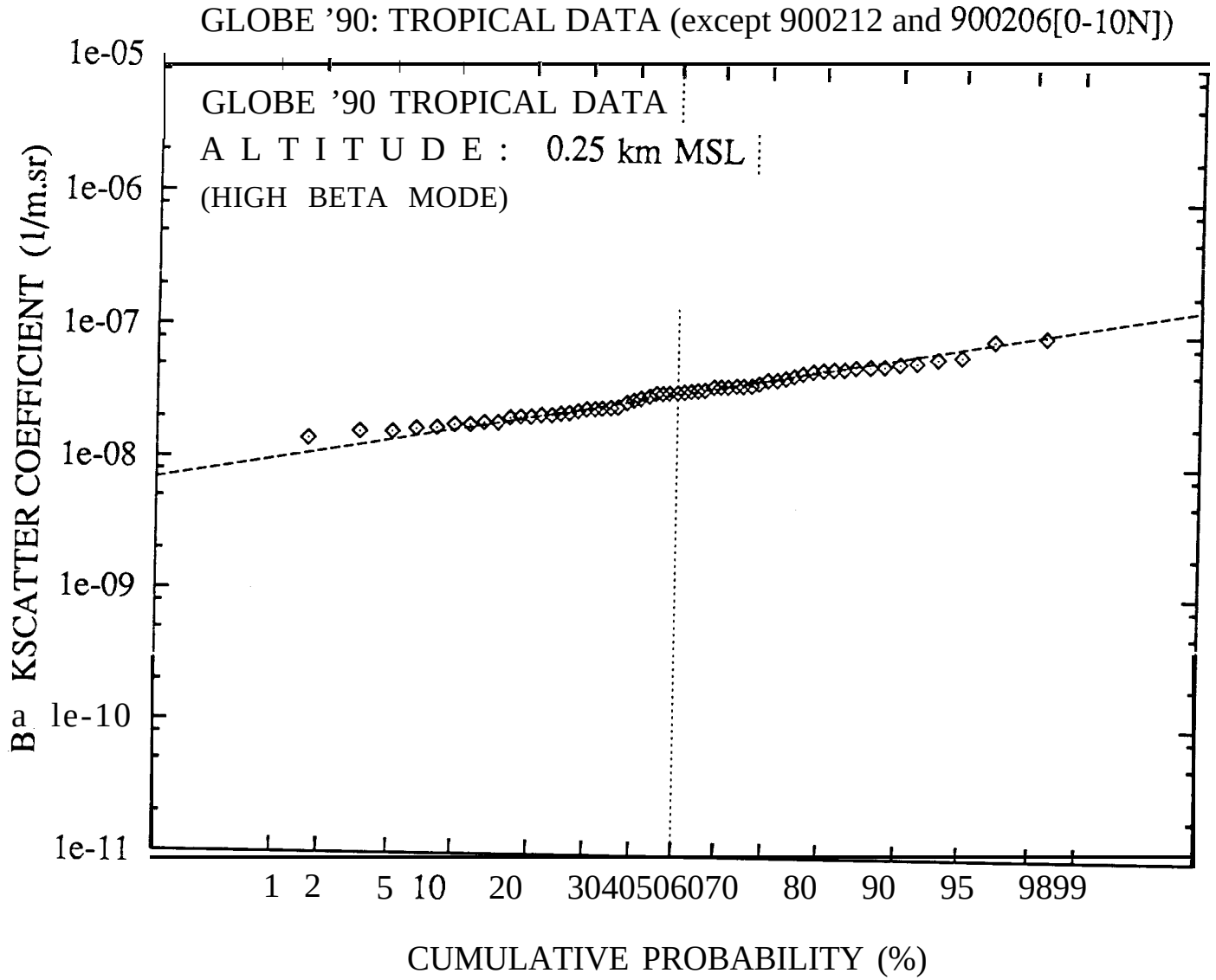
GLOBE '90: TROPICAL DATA (except 900212 and 900206[0-10N])
GLOBE '90 TROPICAL DATA
ALTITUDE: 0.25 km MSL
(HIGH BETA MODE)
1e-05
1e-06
1e-07
1e-08
1e-09
1e-10
1e-11
Ba KSCATTER COEFFICIENT (1/m.sr)
1 2 5 10 20 30 40 50 60 70 80 90 95 98 99
CUMULATIVE PROBABILITY (%)

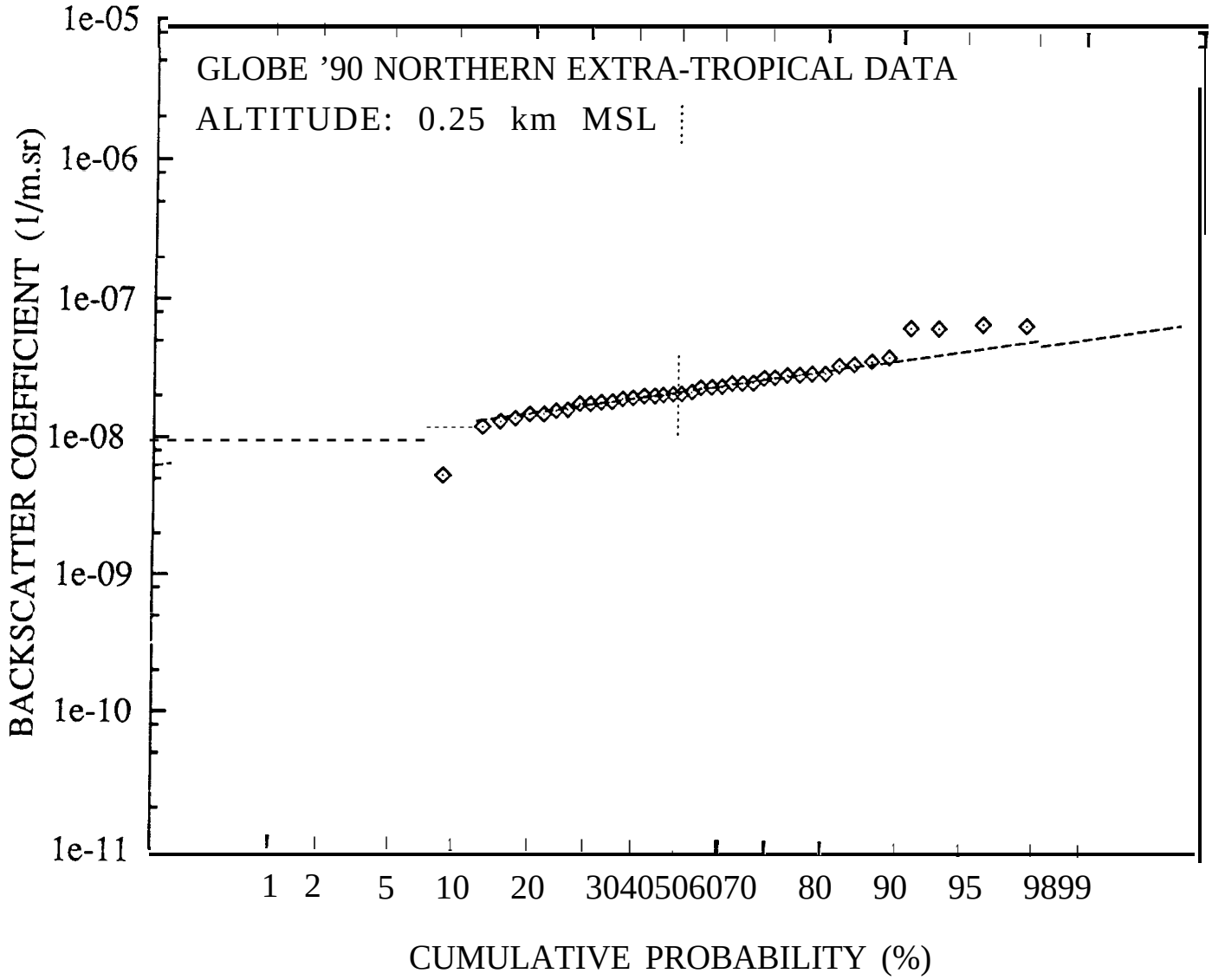
GLOBE '90 NORTHERN EXTRA-TROPICAL DATA
ALTITUDE: 0.25 km MSL
BACKSCATTER COEFFICIENT (1/m.sr)
1e-05
1e-06
1e-07
1e-08
1e-09
1e-10
1e-11
1 2 5 10 20 3040506070 80 90 95 9899
CUMULATIVE PROBABILITY (%)

3/18/96

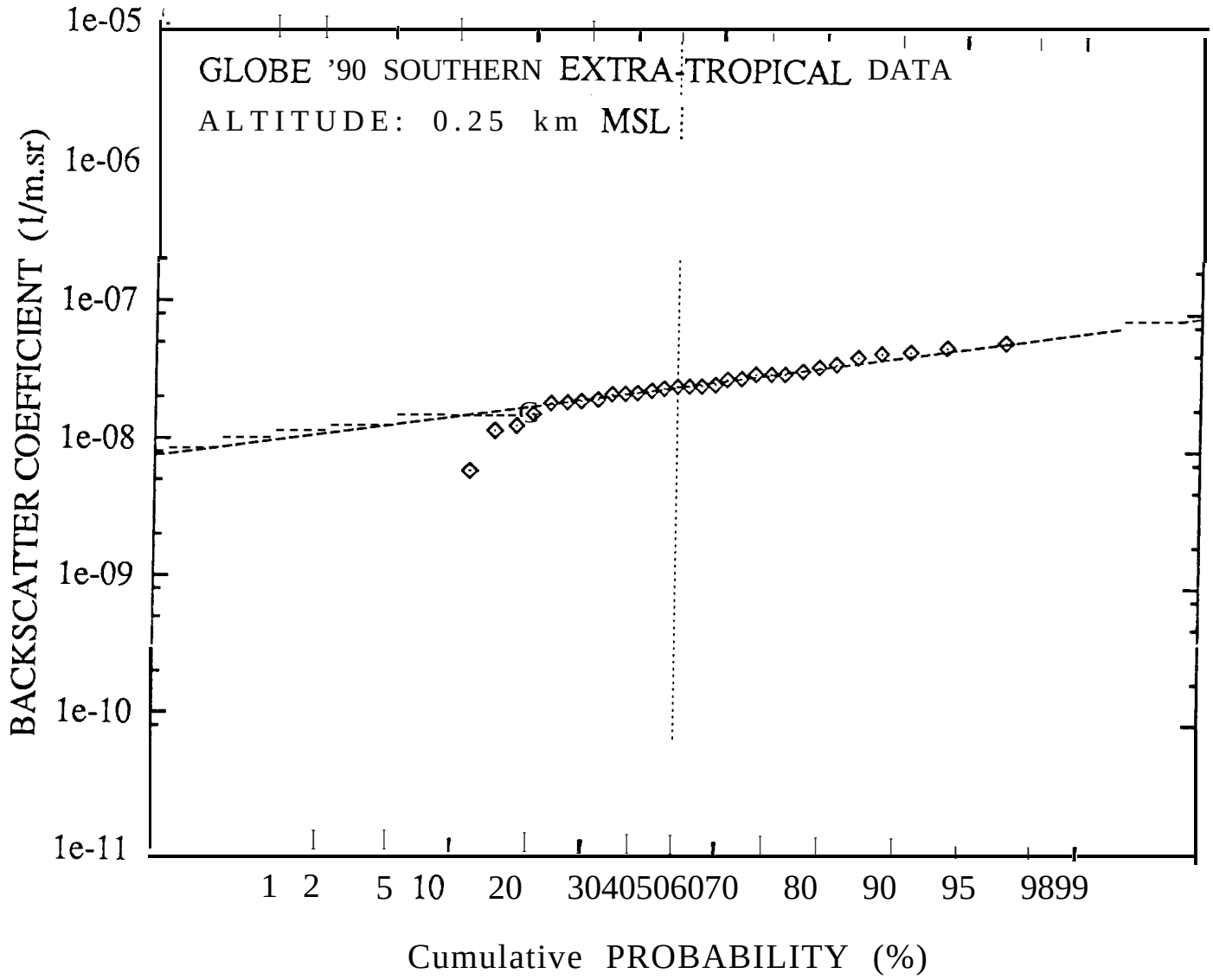
GLOBE '90 SOUTHERN EXTRA-TROPICAL DATA
ALTITUDE: 0.25 km MSL
BACKSCATTER COEFFICIENT (1/m.sr)
1e-05
1e-06
1e-07
1e-08
1e-09
1e-10
1e-11
1 2 5 10 20 30 40 50 60 70 80 90 95 98 99
Cumulative PROBABILITY (%)

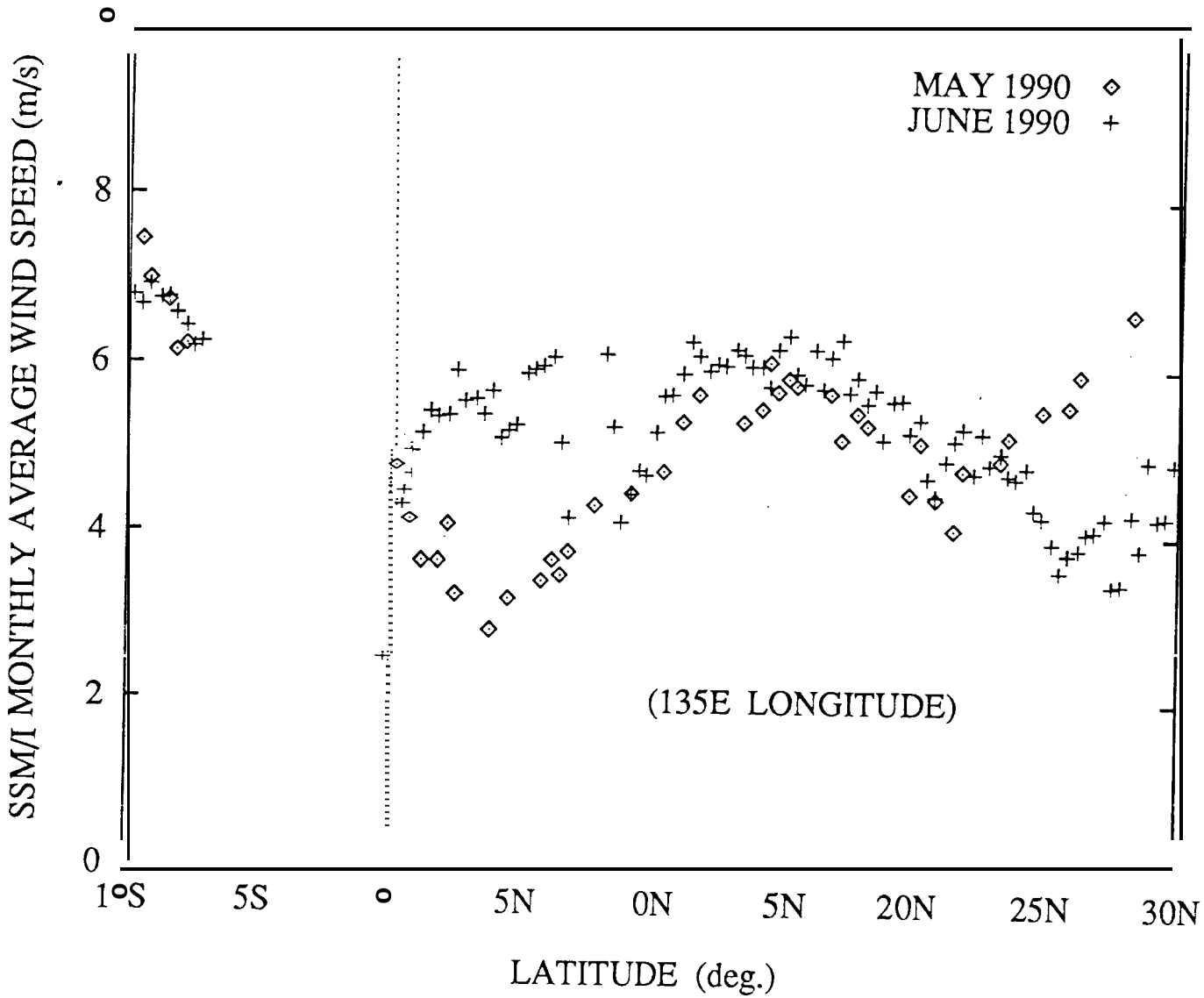
SSM/I MONTHLY AVERAGE WIND SPEED (m/s)
0
2
4
6
8
MAY 1990
JUNE 1990
(135E LONGITUDE)
1°S
5S
0
5N
0N
5N
20N
25N
30N
LATITUDE (deg.)

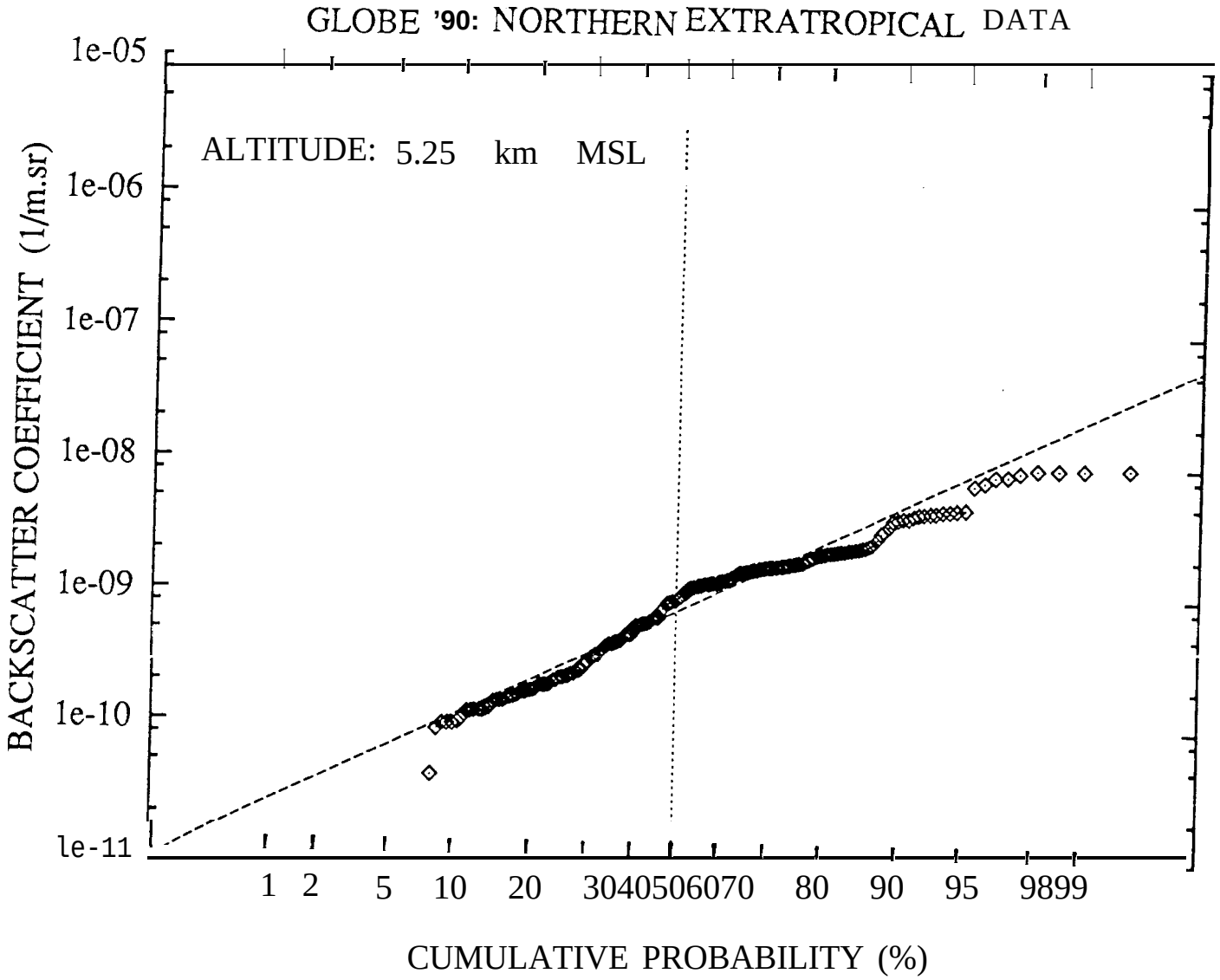
GLOBE '90: NORTHERN EXTRATROPICAL DATA
ALTITUDE: 5.25 km MSL
BACKSCATTER COEFFICIENT (1/m.sr)
1e-05
1e-06
1e-07
1e-08
1e-09
1e-10
1e-11
1 2 5 10 20 30 40 50 60 70 80 90 95 98 99
CUMULATIVE PROBABILITY (%)

Fig 13